DOKUZ EYLÜL UNIVERSITY
GRADUATE SCHOOL OF NATURAL AND APPLIED SCIENCES

FRACTURE BEHAVIOR OF WELDED MIS-MATCHED JOINTS

by
Uygar ÇEVİK

August, 2008
İZMİR

FRACTURE BEHAVIOR OF WELDED MIS-MATCHED JOINTS

A Thesis Submitted to the Graduate School of Natural Sciences of Dokuz Eylül University in Partial Fulfillment of the Requirements for the Degree of Master of Science in Mechanical Engineering, Mechanics Program

by

Uygar ÇEVİK

August, 2008

İZMİR

M.Sc THESIS EXAMINATION RESULT FORM

We have read the thesis entitled **"FRACTURE BEHAVIOR OF WELDED MIS-MATCHED JOINTS"** completed by **UYGAR ÇEVİK** under supervision of **ASSISTANT PROFESSOR DR. ÇINAR EMİNE YENİ** and we certify that in our opinion it is fully adequate, in scope and in quality, as a thesis for the degree of Master of Science.

Assist. Prof. Dr. Çınar Emine YENİ

_____

Supervisor

……. …….

_____ _____

(Jury Member) (Jury Member)

_____

Prof.Dr. Cahit HELVACI

Director

Graduate School of Natural and Applied Sciences

ACKNOWLEDGEMENTS

I would like to gratefully acknowledge the helpful encouragement and guidance I received throughout my study from my advisor Assist. Prof. Dr. Çınar Emine Yeni.

I would also like to thank my family and my friends for their love, encouragement and constant moral support; their contribution makes it all worthwhile.

Uygar ÇEVİK

FRACTURE BEHAVIOR OF WELDED MIS-MATCHED JOINTS

ABSTRACT

In this study, laser beam welded Aluminum Alloy 6056 plates have been used to obtain the crack resistance curves (R-curves) in Compact Tension C(T) specimens. Laser beam welding is a noval joining method used for hard to join materials, such as aluminum alloys, which were considered unweldable formerly. Defect free welds have been obtained with Nd: YAG type laser. Three types of C(T) specimens have been employed for this study, namely, Base Metal (BM), welded specimen with crack in the Weld Metal (WM) and welded specimen with crack in the Heat Affected Zone (HAZ). Fracture mechanics test have been carried out in order to determine the Crack Tip Opening Displacement (CTOD), Crack Mouth Opening Displacement (CMOD) and crack extension (Δa) values corresponding to the applied load. ABAQUS software has been utilized to carry out the numerical analysis. The input parameters were the applied load and the crack length. The output parameters were CTOD, CMOD and *J*-Integral. Experimental and numerical results have been compared with various graphics, it can be concluded that they are in good agreement for all conditions.

Keywords: J-Integral, R-Curve, Crack Tip Opening Displacement (CTOD), Elastic Plastic Fracture Mechanics (EPFM), Laser Welding, Aluminum Alloys

MUKAVEMET UYUŞMAZLIĞI OLAN KAYNAKLI BAĞLANTILARIN KIRILMA DAVRANIŞI

ÖZ

Bu çalışmada, kompakt çekme C(T) numunelerinde direnç eğrilerini (R-eğrisi) elde etmek için lazer kaynaklı alüminyum alaşım 6056 plakalar kullanılmıştır. Lazer ışın kaynağı, klasik yöntemlerle kaynak yapılması mümkün olmayan alüminyum alaşımlar gibi malzemeler için yeni geliştirilmiş bir birleşme metodudur. Bu çalışmada kaynak Nd: YAG tipi lazer ile yapılmıştır. Çalışma için üç tip çekme numunesi kullanılmıştır: Ana Metal (BM), kaynaklanmış Kaynak Metali'nde çatlak bulunduran numune (WM) ve Isıdan Etkilenmiş Bölge'de (HAZ) çatlak bulunduran numune. Kırılma mekaniği testi, uygulanan yüke bağlı olarak Çatlak Ucu Açılma Yerdeğiştirmesi (CTOD), Çatlak Ağzı Açılma Yerdeğiştirmesi (CMOD) ve Çatlak İlerlemesi (Δa) değerlerini belirlemek için yapılmıştır. Nümerik analizler için ABAQUS programı kullanılmıştır. Girdi parametreleri, uygulanan yük ve çatlak uzunluğu, çıktı parametreleri ise CTOD, CMOD ve *J*-integrali olarak alınmıştır. Deneysel ve nümerik sonuçlar çeşitli grafiklerle karşılaştırılmış ve bu sonuçların bütün durumlar için iyi bir uyum gösterdiği görülmüştür.

Anahtar Kelimeler: J-İntegrali, R-Eğrileri, Çatlak Ucu Açılma Yerdeğiştirmesi, Elastik Plastik Kırılma Mekaniği (EPKM), Lazer Kaynağı, Aluminyum Alaşımlar

CONTENTS **Page**

CHAPTER ONE
INTRODUCTION

1.1 Laser Welding

Almost 20 years ago, laser welding was in its infancy and used primarily for exotic applications where no other welding process would be suitable. Today, laser welding is a full-fledged part of the metalworking industry, routinely producing welds for common items such as cigarette lighters, watch springs, motor/transformer lamination, hermetic seals, battery and pacemaker cans, hybrid circuit packages and also in automotive and aerospace applications. Yet not enough manufacturing engineers have seriously considered employing lasers in their own operations.

Why? There are many reasons, but a primary one must be an unfamiliarity with the operation and capabilities of a laser system. Other reasons, such as a relatively high initial cost and a concern about using lasers in the manufacturing environment, also are frequently cited.

Laser welding could be used in place of many different standard processes, such as resistance (spot or seam), submerged arc, RF induction, high-frequency resistance, ultrasonic and electron-beam welding. While each of these techniques has established an independent niche in the manufacturing world, the versatile laser welding approach has the ability to operate efficiently and economically in many different applications. Its versatility will even permit the welding system to be used for other machining functions, such as cutting, drilling, scribing, sealing and serializing.

Actually, there are many benefits laser welding can offer to manufacturing engineers. Some industry observers state that there are already 2,000 laser machine tools being used for cutting, welding and drilling and that the number could reach 30,000 over the next 15 years as manufacturing engineers become more aware of the

capabilities of lasers. While most laser applications are dedicated to one product or process that involves high-volume, long-run manufacturing, the versatility of a laser to supply energy to hard-to-reach spots, vary the output energy over a wide range, operate under the control of computers and robots and put minimum heat into the part, makes laser welding ideal for many flexible manufacturing operations.

Advantages of laser welding over other conventional welding techniques are presented in Table 1.1.

Table 1.1. Advantages of Laser Welding Compared to Other Processes

Competing Process	**Advantages of Laser Welding**
Gas Metal Arc	Faster welding rates by an order of magnitude; low distortion; no filler metal required; single-pass two-side welding
Submerged Arc	Faster welding rates; low distortion; no flux or filler needed
Resistance Welding	Non-contact, eliminating any debris buildup; can reach otherwise inaccessible locations; faster welding rates
Electron Beam	Does not need to be performed in a vacuum; on-line processing; shorter cycles and higher uptimes; welds magnetic materials; does not require radiation shielding

Welding results when materials are heated to a molten state as in fusion welding techniques or while they are still in solid state as in friction stir welding. Lasers generate light energy that can be absorbed into materials and converted to heat energy. By employing a light beam in the visible or infrared portion of the electromagnetic spectrum, we can transmit this energy from its source to the material, using delivery optics which can focus and direct the energy to a very small, precise point. Since the laser emits coherent radiation, the beam of energy has minimal divergence and can travel large distances without significant loss of beam quality or energy.

What does all this mean to the manufacturing engineer? To appreciate the potential of employing lasers in welding operations, some of the traditional

approaches must be redefined in order to view "efficiency", as it relates to energy conversion. The laser is a relatively inefficient converter of electrical energy into output light, with the best lasers achieving only 2 to 15 percent energy conversion, depending upon the type of laser being used. However, virtually all of this output light energy is delivered to a small spot, as small as a few hundreds of a milimeters or less.

Consequently, for applying thermal energy to small areas, there are no other methods as efficient as lasers. This ability to selectively apply energy offers some distinctive metallurgical advantages in some welding applications, but also creates some unique problems. Since the surface heating generated by the laser light relies upon the material's heat conductivity to produce the weld, penetration is usually limited to less than 10 millimeters. By using a technique known as "key holing," higher power lasers (>106 W/cm²) can make deeper penetrations.

By heating the spot of laser focus above the boiling point, a vaporized hole is formed in the metal. This is filled with ionized metallic gas and becomes an effective absorber, trapping about 95 percent of the laser energy into a cylindrical volume, known as a keyhole. Temperatures within this keyhole can reach as high as 25,000°C, making the key holing technique very efficient. Instead of heat being conducted mainly downward from the surface, it is conducted radially outward from the keyhole, forming a molten region surrounding the vapor. As the laser beam moves along the work-piece, the molten metal fills in behind the keyhole and solidifies to form the weld. This technique permits welding speeds of hundreds of centimeters per minute or greater, depending on laser size.

1.2 Laser Welding Process Principles

Generally, there are two types of lasers that are being used for welding operation: CO_2 and Nd:YAG.

Both CO_2 and Nd:YAG lasers operate in the infrared region of the electromagnetic radiation spectrum, invisible to the human eye. The Nd:YAG provides its primary light output in the near-infrared, at a wavelength of 1.06 microns. This wavelength is absorbed quite well by conductive materials, with a typical reflectance of about 20 to 30 percent for most metals. The near-infrared radiation permits the use of standard optics to achieve focused spot sizes as small as 0.25 mm in diameter.

On the other hand, the far infrared (10.6 micron) output wavelength of the : CO_2 laser has an initial reflectance of about 80 percent to 90 percent for most metals and requires special optics to focus the beam to a minimum spot size of 0.75 to 1 mm diameter. However, whereas Nd:YAG lasers might produce power outputs up to 500 watts, : CO_2 systems can easily supply 10,000 watts and greater.

As a result of these broad differences, the two laser types are usually employed for different applications. The powerful: CO_2 lasers overcome the high reflectance by key holing, wherein the absorption approaches blackbody. The reflectivity of the metal is only important until the keyhole weld begins. Once the material's surface at the point of focus approaches its melting point, the reflectivity drops within microseconds.

1.3 Laser Welding Calculations

Knowing the size of the focused spot is helpful in calculating energy density at the work surface. In performing a laser weld, optics to focus the laser beam to the desired size are necessary.

For a fundamental mode (TEM_{00}) beam:

$$S = (4l / p) \times (F / D) \tag{1.1}$$

where:

S = Focused Spot Diameter

l = Laser Wavelength

F = Focal Length of Objective Lens

D = Diameter of Laser Beam

For a multimode beam:

$$S = F \times f \tag{1.2}$$

where:

F = Focal Length of Objective Lens

M = Laser Beam Divergence

If one assumes the part to be welded as a semi-infinite solid, with a constant incident heat flux, then the temperature distribution as a function of depth into the material is given by:

$$T(x,t) = (2E/K) \times \left[(kt/p)^{1/2} \times \exp(-x^2/4kt) - (x/2)\, erfc\left(x/2(kt)^{1/2}\right) \right] \tag{1.3}$$

where:

$T(x,t)$=Temperature at a distance x below the work surface, at a time t after start of constant heat input

E = constant heat flux input

K = thermal conductivity

k = thermal diffusivity

x = depth below surface

t = time after start of heat flux input

$erfc$ = complimentary error function

and at the surface $x = 0$, the temperature rise will be:

$$T(x,t)_{x=0} = (2E/K) \times (kt/p)^{1/2} \quad (1.4)$$

1.4 Characteristics of the Laser Beam

The main characteristics of the laser beam can be listed as follows:

1.4.1 Monochromatic

All of the photons which compose the beam are of the same energy and therefore the same wavelength. If the laser beam was directed through an optical prism it could not split up into the separate colors representing the wavelengths of the optical spectrum.

1.4.2 Coherent

The light waves are in phase (in step). The meaning of "coherent" light is as follows: Light moves in the form of a wave, with crests and troughs. Like all other kinds of electromagnetic radiation, it can be characterized both by its frequency, or number of wave crests passing a given point per second, and by its wavelength, or distance between wave crests. (Beams of such radiation travel through a vacuum at the highest velocity anything can achieve; see relativity.) Different wavelengths of light are seen as different colors.

1.4.3 Culminated

The laser beam does not diverge. It can be projected great distances without significant spreading. For example, it is used for topographical surveys where elevations miles away can be measured from a single, central location. Culmination makes is possible for laser beams to target satellites, etc. at great distance.

Because of these three characteristics the laser beam can be precisely focused to very small diameters, resulting in an enormous increase in energy density**.**

1.5 Laser Welding Factors

Thermal diffusivity, mentioned in the above calculations, is a measure of the ability of the material to conduct heat. The lower the diffusivity, the more the heat remains in the vicinity of the laser beam spot.

Metals with low boiling points produce a large amount of metal vapor which could initiate gas breakdown and plasma generation in the region of high beam intensity just above the metal surface. This plasma, which readily absorbs the laser energy, can block the passing beam, and bubbles tend to form at the root of the weld. If the viscosity is high, these bubbles do not escape before the molten metal solidifies.

Although the melting point of metals does not have a significant effect on laser weldability, it must be reached during the initial absorption of energy. Thus, low melting point materials are easier to weld with a laser than high melting point metals.

1.6 Metallurgical Considerations

The effect of welding on various materials depends upon many of their metallurgical properties such as "hot strength." After the applied energy is removed, the melt pool solidifies and then it slowly cools to the same temperature as the surrounding material. During this cooling, the material contracts, creating tensile stresses in the fusion zone. Materials that have a low tensile strength at temperatures near their melting point are said to exhibit "hot shortness," which often results in cracks appearing in the weld.

Similarly, other thermal transformations, such as the martensitic transformation of high carbon steel, also can lead to cracking in or near the weld. To overcome this

tendency, special precautions such as pre- and post-welding heating of the material is necessary. However, virtually no thermal distortion occurs during laser welding. The lower heat input requirement has other benefits, such as being able to use fixtures that do not need to withstand large thermal expansion forces or to act as heat sinks.

Chemical reactions, such as oxidation or nitriding, with atmospheric gases at high temperatures can pose problems, particularly when the oxides or other elements formed have disassociation temperatures far above the melting point of the metal. The result is brittle, porous welds. Covering the welding area with an inert gas such as argon or helium minimizes these reactions in most cases. For some materials, it may be necessary to weld within a sealed chamber to prevent outside contamination.

1.7 Laser Welding Approaches

There are two different approaches to laser welding. One is the low-power method for relatively thin materials; and the other is the "brute force" high-power approach that generally involves key holing. In both cases, since filler material is rarely used, a tight fitup of the parts being welded is necessary. For butt and seam welds, the laser energy is applied to the junction of the materials, minimizing heat input and distortion and permitting high processing speeds.

For lap joints, the tolerances for seam alignment are somewhat looser. The width of the weld is the major consideration. The upper material forms most of the fusion zone so that a good laser-weldable material could be welded to less suitable material by putting the former material on top.

1.8 Evaluating Laser Welding Systems

The two laser types being used for laser welding, namely CO_2 and Nd:YAG, can operate in either the continuous or the pulsed mode. CO_2 lasers, which range in power from 50 to 15,000 watts, are more efficient in their conversion of electrical power to laser radiation than Nd:YAG lasers, which range from about 50 to 800

watts output power. However, as mentioned above, the reflectivity of most metals is much higher at the CO_2 wavelength than the Nd:YAG wavelength.

Recent advances in fast-axial-flow CO_2 lasers provide improved beam characteristics, making these systems competitive with electron beam welding for deep-penetration applications. Fast-spiral-flow CO_2 lasers now are able to produce fundamental-mode outputs in the kilowatt range, which gives higher energy densities suitable for welding thermally sensitive alloys or materials where thermal distortion is a problem.

Slow-axial-flow lasers with enhanced pulsed capabilities offer an advantage over fast-axial-flow units for applications requiring rapid energy coupling and low heat input. In pulsed operation, the peak power in the pulse is several times greater than the continuous-wave power, although the average power is lower. This peak power overcomes surface reflectivity and minimizes thermal damage to the surrounding material.

Solid state lasers (the generic name for Nd:YAG, Nd:Glass and similar lasers), are preferred for low- to moderate- power applications. They have found extensive applications in the electronic/electrical industries for spot welding and beam lead welding integrated circuits to thin film interconnecting circuits on a substrate.

One consideration that can be important in evaluating laser welding is the physical size of the equipment. Solid state laser welding systems are relatively small compared to CO_2 systems, which could occupy an average room to achieve the high powers required. For delicate welding operations, such as welding lamp filaments, the solid state welding systems offer the advantage of coaxial viewing optics. Since the wavelength of the Nd:YAG laser is close to the visible spectrum, standard lenses can transmit both the laser light and the image of the workpiece.

1.9 Aluminum and its Alloys

Aluminum is a silverish white metal that has a strong resistance to corrosion and like gold, is rather malleable. It is a relatively light metal compared to metals such as steel, nickel, brass, and copper with a specific gravity of 2.7. Aluminum is easily machinable and can have a wide variety of surface finishes. It also has good electrical and thermal conductivities and is highly reflective to heat and light.

At extremely high temperatures (200-250°C) aluminum alloys tend to lose some of their strength. However, at subzero temperatures, their strength increases while retaining their ductility, making aluminum an extremely useful low-temperature alloy.

Aluminum alloys have a strong resistance to corrosion which is a result of an oxide skin that forms as a result of reactions with the atmosphere. This corrosive skin protects aluminum from most chemicals, weathering conditions, and even many acids, however alkaline substances are known to penetrate the protective skin and corrode the metal.

Aluminum also has a rather high electrical conductivity, making it useful as a conductor. Aluminum connectors have a tendency to become loosened after repeated usage leading to arcing and fire, which requires extra precaution and special design when using aluminum wiring in buildings.

Aluminum is a very versatile metal and can be cast in any form known. It can be rolled, stamped, drawn, spun, roll-formed, hammered and forged. The metal can be extruded into a variety of shapes, and can be turned, milled, and bored in the machining process. Aluminum can be riveted, welded, brazed, or resin bonded. For most applications, aluminum needs no protective coating as it can be finished to look good, however it is often anodized to improve color and strength.

1.9.1 Classification of Aluminum Alloys

Classification of aluminum alloys is established by the International Alloy Designation System (IADS), based on the classification developed by Aluminum Association of the United States. This classification is accepted by most countries.

1.9.1.1 Classification of Wrought Aluminum Alloys

Each wrought aluminum alloy is designated by a four digit number. The first digit indicates the alloy group according to the major alloying element. The second digit indicates modification of the alloy or impurity limits. Original (basic) alloy is designated by "0" as the second digit. Numbers 1…9 indicate various alloy modifications with slight differences in the compositions:

Table 2.1. Classification of Wrought Aluminum Alloys

Alloy Designation	**Alloying Elements**
1xxx	Aluminum 99.0% minimum
2xxx	Copper (1.9%...6.8%)
3xxx	Manganese (0.3%...1.5%)
4xxx	Silicon (3.6%...13.5%)
5xxx	Magnesium (0.5%...5.5%)
6xxx	Magnesium and Silicon (Mg 0.4%...1.5%, Si 0.2%...1.7%)
7xxx	Zinc (1%...8.2%)
8xxx	Others

In the alloys of the 1xxx series the second digit indicates modifications in impurity limits: 0 means natural impurity limit, 1…9 indicate special control of one or more impurities or alloying element. For example:

1070 or 1170 mean minimum 99.70% of aluminum in the alloys, 1050 or 1250 mean 99.50% of aluminum in the alloys, 1100 or 1200 mean minimum 99.00% of aluminum in the alloys.

In all other groups of aluminum alloys (2xxx through 8xxx) the last two digits signify different alloys in the group.

1.9.1.2 Classification of Cast Aluminum Alloys

Each cast aluminum alloy is designated by a four digit number with a decimal point separating the third and the forth digits. The first digit indicates the alloy group according to the major alloying element. The second two digits identify aluminum alloy or indicate the alloy purity:

Table 2.2. Classification of Cast Aluminum Alloys

Alloy Designation	**Alloying Elements**
1xxx	Aluminum 99.0% minimum
2xxx	Copper (4%...4.6%)
3xxx	Silicon (5%...17%) with added copper and/or magnesium
4xxx	Silicon (5%...12%)
5xxx	Magnesium (4%...10%)
7xxx	Zinc (6.2%...7.5%)
8xxx	Tin
9xxx	Others

In the alloys of the 1xx.x series the second two digits indicate the level of purity of the alloy – they are the same as the two digits to the right of the decimal point in the minimum concentration of aluminum (in percents): 150.0 means minimum 99.50% of aluminum in the alloy, 120.1 means minimum 99.20% of aluminum in the alloy.

In all other groups of aluminum alloys (2xx.x through 9xx.x) the second two digits signify different alloys in the group.

The last digit indicates the product form: casting (designated by “0”) or ingot (designated by “1” or “2” depending on chemical composition limits.)

A modification of the original alloy or impurity limits is indicated by a serial letter before the numerical designation. The serial letters are assigned in alphabetical order starting with A but omitting I, O, Q, and X (the letter “X” is reserved for experimental alloys).

1.9.2 Wrought Aluminum Alloys 6xxx Series (Aluminum–Magnesium–Silicon)

6xxx series aluminum alloys include magnesium (Mg) and silicon (Si) as the major alloying elements and copper (Cu), manganese (Mn), chromium (Cr), zinc (Zn), boron (B), lead (Pb) and bismuth (Bi) may be added to these alloys as minor alloying elements.

Alloys in the 6xxx series contain silicon and magnesium approximately in the proportions required for formation of magnesium silicide (Mg2Si), thus making them heat treatable. Although not as strong as most 2xxx and 7xxx alloys, 6xxx series alloys have good formability, weldability, machinability, and relatively good corrosion resistance, with medium strength.

Alloys in this heat-treatable group may be formed in the T4 temper (solution heat treated but not precipitation heat treated) and strengthened after forming to full T6 properties by presipitation heat treatment.

Aluminum-magnesium-silicon alloys are used in aircraft and automotive applications, in architectural applications and as structural material. Some of the common applications are handrails, drive shafts, automotive frame sections, bicycle frames, tubular lawn furniture, scaffolding, stiffeners and braces used on trucks, boats and many other structural fabrications.

For these heat-treatable alloys, an increased loss in tensile strength and elongation compared to 5000 series alloys was noted for welds tested in the as-welded condition. The reduction in weld tensile strength for the precipitation-hardened alloys was caused by the re-solution of precipitates and/or strain hardening in weld metal. The HAZ also was softened by overaging during welding. The hardness results showed that the hardness value decreased 25 percent compared to the parent material [Vickers Hardness (Hv)150 for the parent material, Hv113 for the HAZ, and Hv110 for the weld metal].

The tensile failure strengths of the 1.6-millimeter-thick 6082 aluminum alloy were generally between 85 and 90 percent of the base metal strength for the autogenous and wire feed welds (using aluminum-silicon 4043A and aluminum-magnesium 5556A filler), with elongation to failure of 4 to 12 percent. The elongation-to-failure values for welds made with 4043A wire were low compared to the 5556A wire.

CHAPTER TWO
FRACTURE MECHANICS

2.1 Introduction to Fracture Mechanics

Through the ages the application of materials in engineering design has posed difficult problems to mankind. In the Stone Age, the problems were mainly in the shaping of the material. In the early days of the Bronze Age and the Iron Age, the difficulties were both in production and shaping. For many centuries metal-working was laborious and extremely costly. Estimates go that the equipment of a knight and horse in the thirteenth century was of the equivalent price of a Centurion tank in World War II.

With the improving skill and metal working, applications of metals in structures increased progressively. Later it was experienced that structures built of these materials did not always behave satisfactorily, and unexpected failures often occurred. Detailed descriptions of castings and forgings produced in the Middle Ages exist. When judged with present day knowledge, these production methods must have been liable to build important technical deficiencies into the structure. This must have made gunners pray-when igniting the charge -that the projectile would be properly delivered and the barrel not blown up.

The vastly increasing use of metals in the nineteenth century caused the number of accidents and casualties to reach unknown levels. The number of people killed in railway accidents in Great Britain was in the order of two hundred per year during the decade 1860-1870. Most of the accidents were a result of derailing caused by fractures of wheels, axles or rails. Anderson has recently made an interesting compilation of accident reports from the last two hundred years. A few quotations follow:

"On the 19th of March 1830 about 700 persons assembled on the Montrose suspension bridge to witness a boat race when one of the main chains gave way... and caused considerable loss of life."

"On the 22nd of January 1866, a portion of the roof of the Manchester railway station fell, causing deaths of two men. The accident was caused by failure of cast-iron struts connected..."

"The failure of a large gas tank in New York occurred on December 13, 1898, killing and injuring a number of people and destroying considerable surrounding property."

"A high pressure water main burst at Boston. January 3, 1913 and flooded the district..,"

"Engineering, February 1866. With some *fifty to sixty* boiler explosions annually in the United Kingdom attended as they are with loss of many lives and destruction of property, is it not time that the Government should appoint a commission to inquire into the subject."

Some of these accidents were certainly due to a poor design, but it was gradually discovered that material deficiencies in the form of pre-existing flaws could initiate cracks and fractures. Prevention of such flaws would improve structural performance. Better production methods, together with increasing knowledge and comprehension of material properties led to a stage where the number of failures was reduced to more acceptable levels.

A new era of accident prone structures started with the introduction of all-welded designs. Out of 2500 Liberty ships built during World War II. 145 broke in two and almost 700 experienced serious failures. The same disaster struck many bridge and other structures. Information on these failures was also given by Anderson and more specifically e.g. by Biggs.

The failures often occurred under conditions of low stresses (several ships failed suddenly while in the harbor) which made them seemingly inexplicable. As a result, extensive investigations were initiated in many countries and especially in the United Sates of America. This work has revealed that here again, flaws and stress concentrations (and to a certain extent internal stresses) were responsible for failure.

The fractures were truly brittle: they were accompanied by very little plastic deformation. It turned out that the brittle fracture of steel was promoted by low temperatures and by conditions of triaxial stress such as may exist at a sharp notch or a flaw. Under these circumstances structural steel can have cleavage fracture without noticeable plastic deformation. Above a certain temperature, called the transition temperature, the steel behaves in a ductile manner. The transition temperature may go up as a result of the heat cycle during the welding process.

At present, brittle fractures of welded structures built out of low strength structural steels can be satisfactorily prevented. It has to be ensured that the material is produced to have a low transition temperature and that the welding process does not raise the ductile-brittle transition. Large stress concentration should be avoided and the welds should be checked to be virtually free of defects.

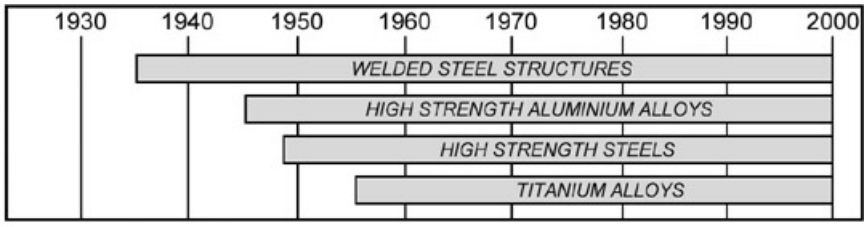

Figure 2.1. Introduction of high strength materials for structural applications

After World War II the use of high strength materials has increased considerably. These materials are often selected to realize weight savings. Simultaneously, stress analysis methods were developed which enable a more reliable determination of local stresses. This permitted safety factors to be reduced resulting in further weight savings. Consequently, structures designed in high strength materials have only low margins of safety. This means that service stresses (sometimes with the aid of an

aggressive environment) may be high enough to induce cracks, particularly if pre-existing flaws or high stress concentrations are present. The high strength materials have a low crack resistance (fracture toughness): the residual strength under the presence of cracks is low. When only small cracks exist, structures designed in high strength materials may fail at stresses below the highest service stresses they were designed for.

Low stress fractures induced by small cracks are, in many aspects, very similar to the brittle fractures of welded low-strength steel structures. Very little plastic deformation is involved; the fracture is brittle in an engineering sense, although the micromechanism of separation is the same as in ductile fracture. The occurrence of low stress fracture in high strength materials induced the development of *Fracture Mechanics.*

Engineering fracture mechanics can deliver the methodology to compensate the inadequacies of conventional design concepts. The conventional design criteria are based on tensile strength, yield strength and buckling stress. These criteria are adequate for many engineering structures, but they are insufficient when there is the likelihood of cracks. Now, after approximately two decades of development, fracture mechanics have become a useful tool in design with high strength materials.

2.2 The Significance of Fracture Mechanics

The object of fracture mechanics is to provide quantitative answers to specific problems concerning cracks in structures. As an illustration, consider a structure containing pre-existing flaws and/or in which cracks initiate in service. The cracks may grow with time owing to various causes (for example fatigue, stress corrosion, creep) and will generally grow progressively faster. The residual strength of the structure, which is the failure strength as a function of crack size, decreases with increasing crack size. After a time the residual strength becomes so low that the structure may fail in service.

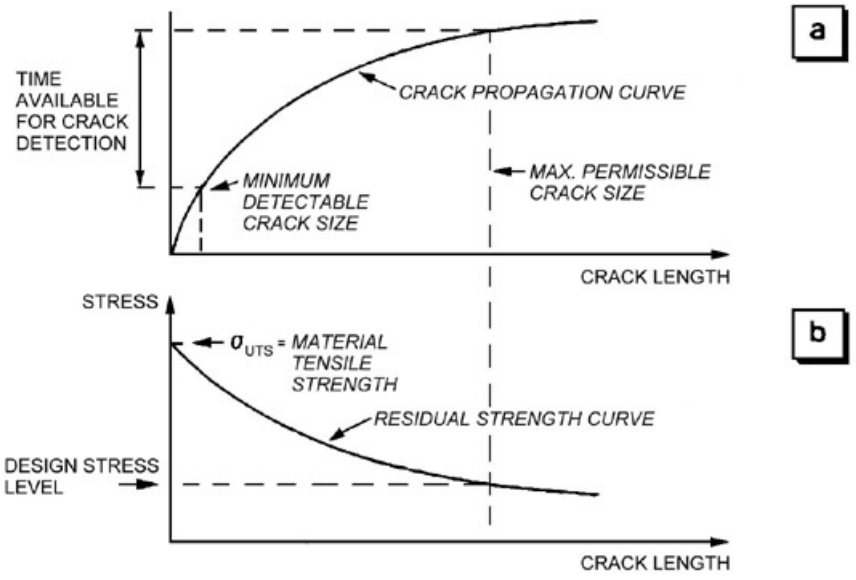

Figure 2.2. The engineering problem of a crack in a structure

With respect to Fig. 2.2, fracture mechanics should attempt to provide quantitative answers to the following questions:

- What is the residual strength as a function of crack size?
- What crack size can be tolerated under service loading, *i.e.* what is the maximum permissible crack size?
- How long does it take for a crack to grow from a certain initial size, for example the minimum detectable crack size, to the maximum permissible crack size?
- What is the service life of a structure when a crack-like flaw (*e.g.* a manufacturing defect) with a certain size is assumed to exist?
- During the period available for crack detection how often should the structure be inspected for cracks?

The field of fracture mechanics is divided into two parts, namely Linear Elastic Fracture Mechanics (LEFM) and Elastic-Plastic Fracture Mechanics (EPFM).

2.3 Fields of Fracture Mechanics

The field of fracture mechanics is divided into two parts, namely Linear Elastic Fracture Mechanics (LEFM) and Elastic-Plastic Fracture Mechanics (EPFM).

2.3.1 Linear Elastic Fracture Mechanics (LEFM)

Linear Elastic Fracture Mechanics (LEFM) first assumes that the material is isotropic and linear elastic. Based on the assumption, the stress field near the crack tip is calculated using the theory of elasticity. When the stresses near the crack tip exceed the material fracture toughness, the crack will grow.

In Linear Elastic Fracture Mechanics, most formulas are derived for either plane stresses or plane strains, associated with the three basic modes of loadings on a cracked body: opening, sliding, and tearing.

Again, LEFM is valid only when the inelastic deformation is small compared to the size of the crack, what we called small-scale yielding.

2.3.2 Elastic Plastic Fracture Mechanics (EPFM)

If the plastic zone ahead of the crack is significantly large then the problem has to be treated elasto-plastically. Due to its complexity the concepts of Elastic-Plastic Fracture Mechanics (EPFM) are not so well developed as LEFM theory, a fact that is reflected in the approximate nature of the eventual solutions.

In 1961 Wells introduced the crack opening displacement (COD) approach. This approach focuses on the strains in the crack tip region instead of the stresses, unlike the stress intensity approach. In the presence of plasticity a crack tip will blunt when it is loaded in tension. Wells proposed to use the crack flank displacement at the tip of a blunting crack, the so-called crack tip opening displacement (CTOD) as a fracture parameter (see figure 2.3.).

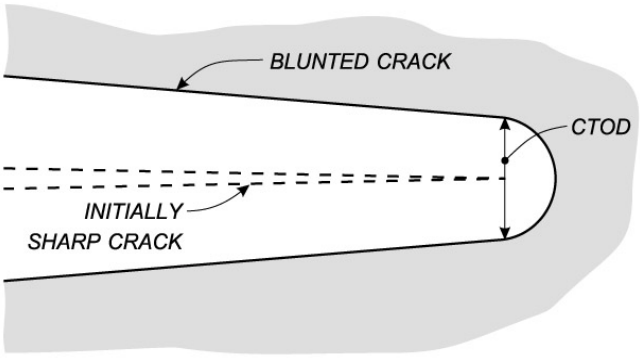

Figure 2.3. Crack tip opening displacement.

Even for tougher materials exhibiting considerable plasticity, critical CTOD values could be defined corresponding to the onset of fracture. Such critical CTOD values could then be used to qualify the materials concerned for a given application. However, initially it proved difficult to determine the required CTOD for a given load and geometry or alternatively to calculate critical crack lengths or loads for a given material.

In 1968 Rice considered the potential energy changes involved in crack growth in non-linear elastic material. Such non-linear elastic behavior is a realistic approximation for plastic behavior, provided no unloading occurs in any part of the material. Rice derived a fracture parameter called *J*, a contour integral that can be evaluated along any arbitrary path enclosing the crack tip. He showed *J* to be equal to the energy release rate for a crack in non-linear elastic material, analogous to G for linear elastic material.

For simple geometries and load cases the *J* integral can be evaluated analytically. However, in practice, finite element calculations are often required. In spite of this, J has found widespread application as a parameter to predict the onset of crack growth in elastic-plastic problems. Later it was found that J could also be used to describe a limited amount of stable crack growth.

2.4 The Crack Tip Opening Displacement (CTOD)

The crack tip opening displacement (CTOD), formerly the crack opening displacement (COD) was first proposed by Wells to describe the fracture behavior in the vicinity of the crack tip. It was conjectured that the opening of the notch faces, namely the crack tip opening displacement, could be used to characterize this behavior. Because CTOD measurements can be made when there is a considerable amount of plastic flow ahead of the crack, this technique may be used to establish critical design stresses or crack sizes in a quantitative manner similar to that of LEFM.

Early in the development of this extension, a check was made to see whether this criterion was in agreement with the existing LEFM formulation. In the case of LEFM, the elastic solution for the opening of the notch faces, 2ν, as a function of x_1 is given by:

$$2\nu = \frac{4\sigma}{E}\left(a^2 - x_1^2\right)^{0.5} \tag{2.1}$$

where the origin of the coordinate system is at the center of the through thickness crack. However, by applying the Irwin plastic zone correction, namely equation (2.1) becomes:

$$2\nu = \frac{4\sigma}{E}\left(\left(a + r_y\right)^2 - x_1^2\right)^{0.5} \tag{2.2}$$

where $a + r_y$ is the effective crack size. The CTOD is found by setting $x_1 = a$ in equation (2.2) and since $r_y \ll a$, it turns out that:

$$\delta = CTOD = \frac{4\sigma}{E}\left(2ar_y\right)^{0.5} = \frac{4K_I^2}{\pi E\sigma_{ys}} \tag{2.3}$$

Equation (4.3) holds in the area of LEFM: fracture occurs at K_{Ic} which is a constant value of CTOD thereby implying that a CTOD fracture criterion applies.

According to Broek, the use of this criterion in LEFM requires the measurement of the CTOD, which is difficult and virtually impossible in a routine test. However, indirectly by substituting equation (2.3) into equation (2.2), and recalling that r_y is small, it follows that:

$$2v = \frac{4\sigma}{E}\left[a^2 - x_1^2 + \left(\frac{E \cdot CTOD}{4\sigma}\right)^2\right]^{0.5} \tag{2.4}$$

By measuring $2v_m$ at $x_1 = 0$, the *Crack Mouth Opening Displacement, (CMOD),* the CTOD may be inferred. It is possible to relate the applied stress to the crack length. For stresses $< 0.75\sigma_{ys}$, a good approximation for CTOD is:

$$\delta = CTOD = \frac{\pi\sigma^2 a}{E\sigma_{ys}} \tag{2.5}$$

which is the same as equation (2.3), apart from a $4/\pi$ factor. In general then:

$$\delta = CTOD = \frac{K_I^2\left(1-\nu^2\right)}{E\lambda\sigma_{ys}} \tag{2.6}$$

where the $\left(1-\nu^2\right)$ factor is deleted for plane stress situations. Various theories have found $1 < \lambda < 2.14$, while direct measurements have yielded λ in the order of unity.

Returning to equation (2.5) or equation (2.6) with $\lambda = 1$, and since $E = \sigma_{ys} / e_{ys}$, it follows that:

$$\frac{\delta}{e_{ys}} = \left(\frac{K_I}{\sigma_{ys}} \right)^2 \tag{2.7}$$

Furthermore, the *elastic strain energy release rate G* becomes in terms of δ:

$$G = \delta \sigma_{ys} \tag{2.8}$$

which, at the onset of crack instability where K_I reaches K_{Ic}, dictates for the elastic case:

$$\frac{\delta_c}{e_{ys}} = \left(\frac{K_{Ic}}{\sigma_{ys}} \right)^2 \tag{2.9}$$

Thus, based solely on a comparison with LEFM techniques, the CTOD approach is compatible with the *K* approach in the plastic regime. It also extends naturally into the elastic-plastic case.

The application of the CTOD approach requires the measurement of δ. After a considerable amount of study, the British Standards Institution adopted BS 5762: "British Standard Methods for Crack Opening Displacement (COD) Testing while, more recently, the ASTM E1290 standard test method for "Crack-Tip Opening Displacement (CTOD) Fracture Toughness Measurement" was accepted. While the test methods and specimens are similar to those specified for K_{Ic} testing, the tests are carried out on a specimen of the material at the thickness of interest. If the thickness is sufficient to give valid K_{Ic} values then the results may be presented in terms of K_{Ic}, if not, they are presented in terms of δ.

Hood indicated that there is a well defined transition temperature effect on the CTOD in slow-bend loading case, while for thicker test specimens or specimens

loaded under impact conditions, the transition temperature is higher and less well defined.

2.5 The *R*-Curve

The *R*-curve is another extension of LEFM into elastic-plastic fracture mechanics. A standard testing procedure with the designation ASTM E 561, was first adopted in 1980. Quoting from this source: "*R* - curves characterize the resistance to fracture during incremental slow- stable crack extension and result from growth of the plastic zone as the crack extends from a sharp notch. They provide a record of the toughness development as a crack is driven stably under increasing crack-extension forces. They are dependent on specimen thickness, temperature, and strain rate." This concept of increasing toughness with slow-stable crack extension, first suggested by Irwin and Kies was the subject of intensive testing and observation in a wide variety of materials during the latter half of the last century. Example of typical force - displacement curves are given in Figure 2.4.

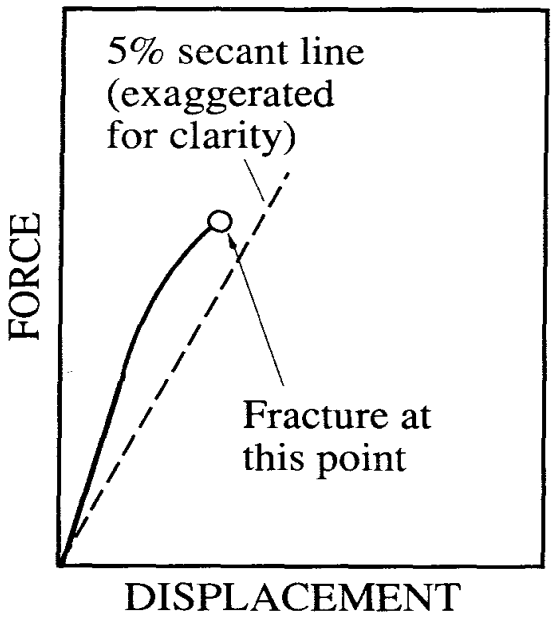

a. Fracture Unstable and Test Record Linear (Brittle)

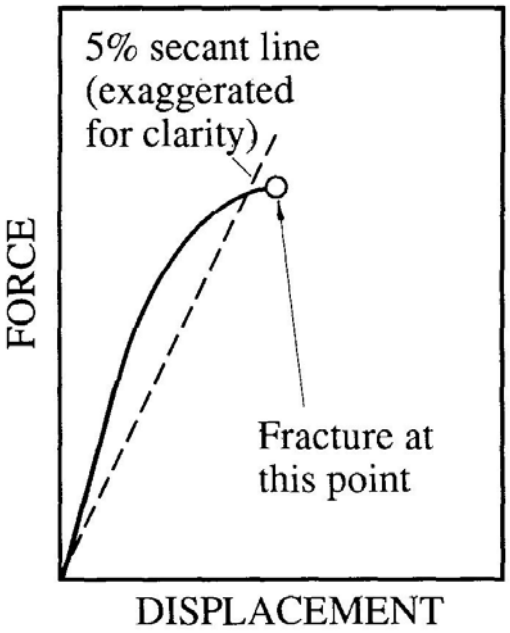

b. Fracture Unstable and Test Record Non-Linear
(Ductile / Brittle)

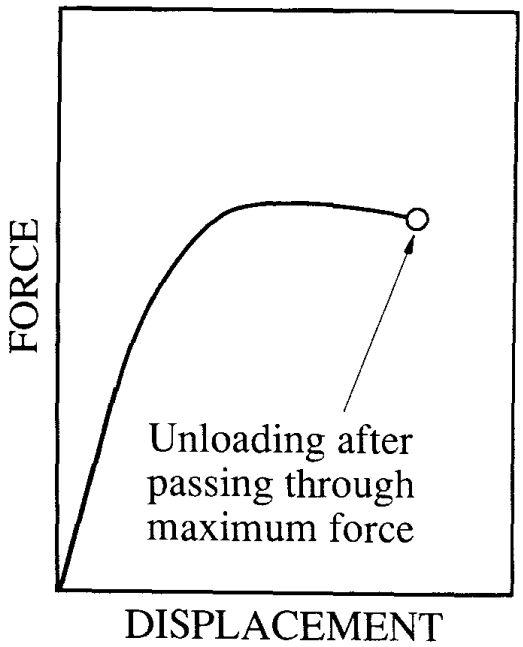

c. Fracture Stable and Test Record Non-Linear
(Ductile)

Figure 2.4 Schematic Force – Displacement Records and Associated Fracture Behavior

The LEFM basis of the *crack growth resistance* concept is that the crack advances under the action of a *crack extension force* and in doing so releases a certain amount of elastic strain energy. According to the Griffith theory, $G = R$, where G is the rate of elastic energy release with respect to crack extension and, hence, is one measure of what are generally known as *crack extension forces*, and R is one measure of a material's *crack growth resistance* and hence the work done to produce a crack increment of δa.

This crack extension force, *G*, is given by the appropriate expression for the particular specimen based on LEFM. In these expressions, the crack length, a, is obtained from measurement procedures of the physical crack size, a_p, the original crack size, a_0, and the effective crack size, a_{eff}, as appropriate to the situation being considered. This crack-extension force may be expressed in terms of another factor, namely, the stress intensity factor:

$$K = \sqrt{G}E \tag{2.10}$$

while, by using the same transformation, a second measure of the crack growth resistance of a material is obtained as:

$$K_R = \sqrt{R}E \tag{2.11}$$

Hence: "During slow-stable fracturing, the developing crack growth resistance, K_R, is equal to the crack extension force, *K*, applied to the specimen. The crack is driven forward by increments of increased load or displacement. Measurements are made at each increment for calculation of *K* values, which are individual data points on the *R*-Curve for the material.

The resulting *R*-curve may be matched with the crack-extension force curves to obtain the critical load necessary for unstable crack propagation. This is accomplished by regarding the *R*-curves as being a function of crack extension, δ_a,

only, i.e., by suppressing their dependency on a_0 and the specimen configuration. The crack-extension force curves for the given configuration may be generated from the appropriate LEFM expression for *K*. The unique curve that is tangent to the *R*-curve defines the critical load that causes unstable fracturing. The value at which this occurs is termed the *plane stress fracture toughness* of the material, and is often given the notation K_C. This condition is indicated mathematically by the relations:

$$\frac{\partial G}{\partial a} = \frac{\partial R}{\partial a}, \qquad G = R \tag{2.12}$$

There are three alternative and somewhat complementary methods of assessing the effective crack length, a_{eff}, used in the determination of K_R. They are: the physical crack length, $a_p = a_0 + \Delta a_p$, where Δa_p is the physical crack growth at one crack tip; a method based upon compliance techniques; and, in the case of C(W) specimen or optionally in the case of C(T) specimens, by a double compliance method first proposed by Heyer and McCabe. Both the effective crack length and load data are used to calculate the *R*-curve in terms of K_R.

For the middle cracked tension, M(T) specimen either of the following and appropriate expressions, may be used to determine the K_R:

$$K_R = \left(\frac{P}{WB}\right)\sqrt{a}\left[1.77 - 0.177\left(\frac{2a}{W}\right) + 1.77\left(\frac{2a}{W}\right)^2\right] \tag{2.13}$$

or:

$$K_R = \left(\frac{P}{WB}\right)\left[\pi a \sec\left(\frac{\pi a}{W}\right)\right]^{0.5} \tag{2.14}$$

where: P is the applied load, B the material thickness, W the width of the specimen, and $a = a_{eff}$ the plastic zone corrected half-crack length.

For the C(T) and C(W) specimens the K_R is determined from:

$$K_R = \left(\frac{P}{B\sqrt{W}} \right) \cdot f\left(\frac{a}{W} \right) \tag{2.15}$$

where:

$$f\left(\frac{a}{W} \right) = \left[\frac{\left(2 + \frac{a}{W} \right)}{\left(1 - \frac{a}{W} \right)^{1.5}} \right] \cdot \left[0.886 + 4.64\left(\frac{a}{W} \right) - 13.32\left(\frac{a}{W} \right)^2 + 14.72\left(\frac{a}{W} \right)^3 - 5.6\left(\frac{a}{W} \right)^4 \right] \tag{2.16}$$

valid for any $a/W \geq 0.35$. In this relation, W is the specimen width measured from the load line, and a the plastic-zone corrected crack length also measured from the load line, i.e., a_{eff}.

2.6 The *J*-Integral

The third extension of LEFM into the field of EPFM, namely the *J*-integral, is discussed on the basis of plastic deformation introduced by Paris. The *J*-integral is seen as a direct extension of the methods of LEFM into the elastic-plastic regime since G cannot be determined from the elastic stress field when there is an appreciable amount of plasticity. Within certain limitations, the *J*-integral does provide a means of determining an energy release rate for cases where plasticity effects are not negligible.

The *J*-integral was proposed by Rice on the basis of variational energy principles as a path independent line integral that characterizes the stress-strain field at the tip of a crack. The original derivation of Rice considered two almost identical bodies

composed of the same linear or non-linear isotropic material, the only difference being that the second body has a flaw whose volume is ΔV greater than the flaw in the first body. In this manner, Rice defined a single valued, path independent integral, known as the J-integral:

$$J = \oint_{\Gamma} \left(W dx_2 - T_i \frac{\partial u_i}{\partial x_1} ds \right), \quad i, j = 1, 2, 3, \tag{2.17}$$

where the strain energy density for a linear or non-linear material is given by:

$$W = \int_0^{\varepsilon_{ij}} \sigma_{ij} de_{ij} \tag{2.18}$$

Within the framework of the *deformation theory of plasticity*, the stress and strain in a plastic or elastic-plastic body are the same as for a nonlinear elastic body, i.e., they have the same stress- strain curve. While strictly applicable in the case where no unloading occurs, it has still been found reasonable even in deliberate unloading cases, such as in fatigue. Hence, under deformation theory and with reference to figure 4.9:

- Γ is a closed contour followed counterclockwise in a stressed solid,
- **T** is the outward drawn tension (traction) vector perpendicular to Γ, where:
    - $T_i = \sigma_{ij} n_j$
    - n_j being the components of the outward unit normal **n** to Γ
- u_i are the displacement in the x_i directions, and
- x_i is an element of Γ

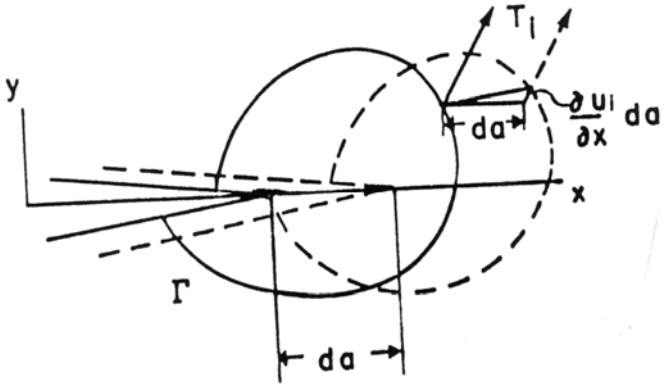

Figure 2.4. Representation of the *J*-integral closed contour.

For a more physical definition, consider J around Γ at a crack tip where crack extension, da, takes place carrying the contour with it. Multiplying both sides of equation (4.18) by da results in:

$\oint W dx_2 da =$ the strain energy gained or lost by moving to the new contour,

and

$\oint T_i \frac{\partial u_i}{\partial x_1} ds da =$ the work done by the tractions on the contour while moving.

As a further physical alternative and in relation to figure 2.5, let's consider a cracked body subjected to a load, P, where δ_p is the work producing component of displacement of the load point. For the nonlinear elastic form of deformation theory, the work done in loading the body, $\int P d\delta_p$, differs for a and $a + da$. This difference is the energy made available for crack extension: or $Jda = AREA$. Hence:

$$J = \frac{AREA}{da} = -\int \frac{\partial P}{\partial a} d\delta_p = \int \frac{\partial \delta_p}{\partial a} dP \qquad (2.19)$$

For the experimental determination of *J*, this equation implies that *J* may be evaluated from load versus load-point-displacement curves for slightly different crack sizes.

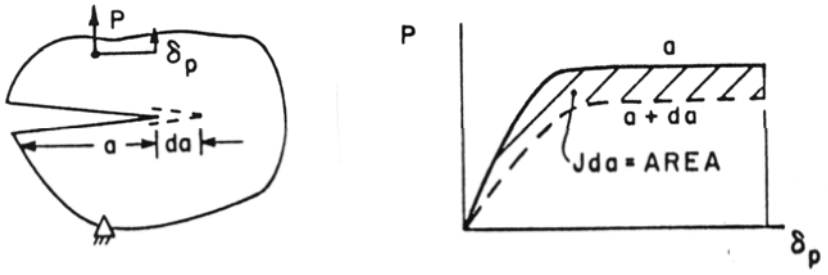

Figure 2.5. A body with a crack subjected to a load.

Although th *J*-integral was originally proposed by Rice as an analytic method of characterizing the crack tip stress and strain fields, Begley and Landes considered a critical value of *J*, namely, J_{Ic}, as a fracture criterion. Again this was an extension of LEFM into the elastic-plastic regime where J_{Ic} may be determined from K_{Ic}.

The definition of J_{Ic} and, indeed, the δ_c and K_c of the CTOD and *R*-curve analyses are illustrated by consideration of the idealized fracture model depicted in table 2.1 and figure 2.6. Initially, a sharp crack is assumed to exist in the body or specimen in its unloaded state. The body is then loaded until the crack tip becomes blunt, views 2 & 3. As the loading increases, the original blunt crack extends into the virgin material, view 4, and the value of *J* at this point is termed the J_{Ic} value. Further loading simply extends the crack into the body.

Table 2.1. A crack-tip schematic of the elastic-plastic process.

Number	Schematic Drawing	Crack Description
1		fatigue crack
2		first loading
3		crack blunting
4		first crack advance, J_{Ic} fracture toughness
5		further crack advance

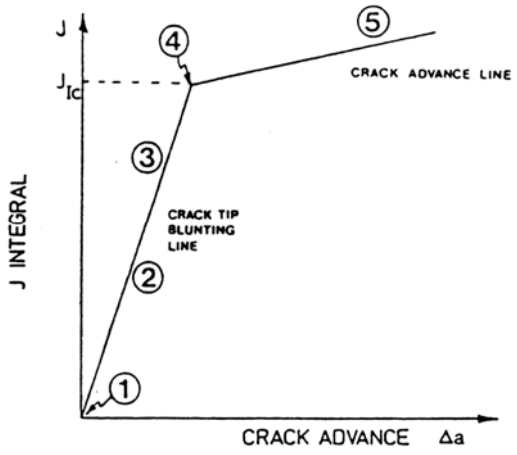

Figure 2.6. An Idealized *R*-Curve for J_{Ic}.

The ASTM E813 and E1152 standards relate to the determination of the J_{Ic} and the *J*-*R*-curve characteristic of materials. Restricting attention, for the most part, to ASTM E813, the ”Standard Test Method for J_{Ic}, A measure of Fracture Toughness” covers the determination of the J_{Ic} fracture toughness near the initiation of slow stable crack growth in metallic materials. Furthermore, while it is not intended to characterize crack growth resistance beyond the initiation of crack extension, it is designed to develop the initial portion of *J*-integral versus crack growth resistance curve (the *J*-*R*-curve of ASTM E1152). J_{Ic} may be used:

- In the field of research and development as a ductile fracture toughness criterion
- In service evaluation, and
- For materials that lack sufficient brittleness or thickness according to the K_{Ic} E399 test.

The area under the load-displacement curve, illustrated in figure 4.14, is determined.

Using the load and displacement scales, this area is converted into the appropriate energy units.

J is calculated according to:

$$J = J_{el} + J_{pl} \tag{2.20}$$

Where J_{el} is the elastic component of J and J_{pl} is the plastic. Specifically, at any particular point $\left(P_i - v_i\right)$ on the load-displacement record, equation (2.20) becomes:

$$J_i = \frac{K_i^2\left(1-\nu^2\right)}{E} + J_{pl(i)} \tag{2.21}$$

where, from E399:

$$K_i = \frac{P_i}{\left(BB_N W\right)^{0.5}} \cdot f\left(\frac{a_0}{W}\right) \tag{2.22}$$

and:

$$J_{pl(i)} = \frac{\eta A_{pl(i)}}{B_N b_0} \tag{2.23}$$

In these expressions:

$A_{pl(i)}$ = area A according to figure 2.7,

B_N = net specimen thickness ($B_N = B$ if no side grooves are present),

b_0 = uncracked ligament, and

$\eta = 2 + 0.522 b_0 / W$.

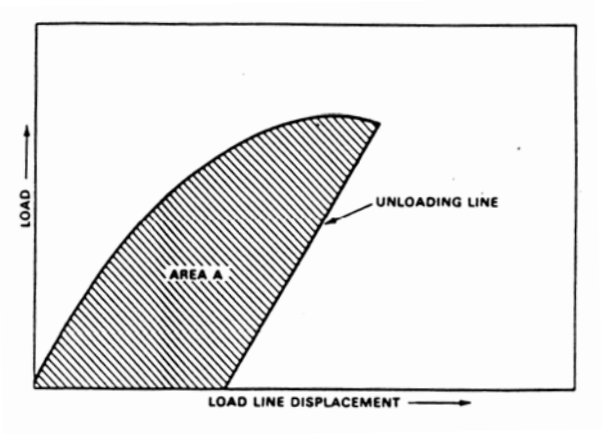

Figure 2.7. Area for J calculation

CHAPTER THREE
INTRODUCTION TO ABAQUS SOFTWARE

3.1 Introduction

ABAQUS is a suite powerful engineering simulation programs, based on the finite element method that can solve problems ranging for relatively simple linear analyses to the most challenging nonlinear simulations. ABAQUS contains an extensive library of elements that can model virtually any geometry. It has an equally extensive list of material models that can simulate the behavior of most typical engineering materials including metals, rubber, polymers, composites, reinforced concrete, crushable and resilient foams, and geotechnical materials such as soils and rock. Designed as a general-purpose simulation tool, ABAQUS can be used to study more than just structural (stress/displacement) problems. It can simulate problems in such diverse areas as heat transfer, mass diffusion, thermal management of electrical components (coupled thermal-electrical analyses), acoustics, soil mechanics (coupled pore fluid-stress analyses), and piezoelectric analysis.

ABAQUS is simple to use even though it offers the user a wide range of capabilities. The most complicated problems can be modeled easily. For example, problems with multiple components are modeled by associating the geometry defining each component with the appropriate material models. In most simulations, even highly nonlinear ones, the user need only provide the engineering data such as the geometry of the structure, its material behavior, its boundary conditions, and the loads applied to it. In a nonlinear analysis ABAQUS automatically chooses appropriate load increments and convergence tolerances. Not only does it choose the values for these parameters, it also continually adjusts them during the analysis to ensure that an accurate solution is obtained efficiently. The user rarely has to define parameters for controlling the numerical solution of the problem.

3.2 The ABAQUS Modules

ABAQUS consist of two main analysis modules: ABAQUS/Standart and AAQUS/Explicit. There are also two special-purpose add-on analysis product for ABAQUS/Standard: ABAQUS/Aqua and ABAQUS/Design. In addition ABAQUS/Safe provides fatigue postprocessing; while ABAQUS/ADAMS, ABAQUS/CAT, ABAQUS/C-MOLD, and ABAQUS/MOLDFLOW are interfaces to ADAMS/Flex, CATIA, C-MOLD, and MOLDFLOW respectively. ABAQUS/CAE is the complete ABAQUS environment that includes capabilities for creating ABAQUS models, interactively submitting and monitoring ABAQUS jobs, and evaluating results. ABAQUS/Viewer is a subset of ABAQUS/CAE that includes just the postprocessing functionality.

3.2.1 ABAQUS/Standard

ABAQUS/Standard is a general-purpose analysis module that can solve a wide range of linear and nonlinear problems involving the static, dynamic, thermal, and electrical response of components.

3.2.2 ABAQUS/Explicit

ABAQUS/Explicit is a special-purpose analysis module that uses an explicit dynamic finite element formulation. It is suitable for short, transient dynamic events, such as impact and blast problems, and is also very efficient for highly nonlinear problems involving changing contact conditions, such as forming simulations. The ABAQUS/CAE interface is the same for both analysis modules. In addition, the output is similar for the two modules, and ABAQUS/Viewer can be used to postprocess the results from either module.

3.2.3 ABAQUS/CAE

ABAQUS/CAE (Complete ABAQUS Environment) is an interactive, graphical environment for ABAQUS. It allows model to be created quickly and easily by producing or importing the geometry of the structure to be analyzed and decomposing the geometry into meshable regions. Physical and material properties can be assigned to the geometry, together with loads and boundary conditions. ABAQUS/CAE contains very powerful options to mesh the geometry and to verify the resulting analysis model. Once the model is complete, ABAQUS/CAE can submit, monitor, and control the analysis jobs. The Visualization module can then be used to interpret the results.

3.2.4 ABAQUS/Viewer

ABAQUS/Viewer is the Visualization module of ABAQUS/CAE; it is an interactive, graphical postprocessor that supports all of the capabilities in the ABAQUS analysis modules and provides a wide range of options for interpreting the results.

3.2.5 ABAQUS/Aqua

ABAQUS/Aqua is a set of optional capabilities that can be added to ABAQUS/Standard. It is intended for the simulation of offshore structures, such as oil platforms. Some of the optional capabilities include the effects of wave and wind loading and buoyancy.

3.2.6 ABAQUS/ADAMS

ABAQUS/ADAMS allows ABAQUS finite element models to be included as flexible components within the MDI ADAMS family of products. The interface is based on the component mode synthesis formulation of ADAMS/Flex.

3.2.7 ABAQUS/CAT

ABAQUS/CAT allows ABAQUS analyses to be set up and postprocessed entirely in CATIA.

3.2.8 ABAQUS/C-MOLD

ABAQUS/C-MOLD translates finite element mesh, material property, and initial stress data from a C-MOLD mold filling analysis to an ABAQUS input file.

3.2.9 ABAQUS/Design

ABAQUS/Design is a set of optional capabilities that can be added to ABAQUS/Standard to perform design sensitivity calculations.

3.2.10 ABAQUS/MOLDFLOW

ABAQUS/MOLDFLOW translates finite element model information from a MOLDFLOW analysis to write a partial ABAQUS input file.

3.2.11 ABAQUS/Safe

ABAQUS/Safe is the fatigue analysis module in ABAQUS. Using results from ABAQUS analyses, it determines the fatigue life of a component.

CHAPTER FOUR
DISPLACEMENT GAUGE SYSTEMS FOR FRACTURE MECHANICS TESTS

4.1. Introduction

Fracture mechanics tests require the determination of two characteristic displacements: the load line displacement V_{LL}, and the crack tip opening displacement (CTOD), δ. For both cases, gauge systems have been developed at GKSS in order to meet the requirements of specific tasks emerging from the research programs.

The load line displacement is needed for determining the deformation energy of a specimen and for evaluating the *J*-integral. Furthermore, V_{LL} may be used for determining crack growth according to the unloading compliance technique. Detailed procedures are given in standards or drafted standards. Although many displacement measuring devices are commercially available, in-house developments turned out to be necessary for three specific cases:

- Measurement of V_{LL} on bend bars using a reference bar in order to avoid including the roller identations in the measruement.
- Measurement of V_{LL} with large working ranges.
- Remote measurement of V_{LL} for high temperature applications using laser beams.

The crack tip opening displacement (CTOD) is a measure of the stresses and strains near the crack tip and can be used to characterize the material's fracture resistance. It can be determined on bend bars by measuring the crack mouth opening displacement at the front face of the specimen and by extrapolating to the crack tip. The same technique can be applied to compact tension C(T) specimens; in this case the displacement at the front face is replaced by V_{LL}.

A technique for measuring the CTOD directly has been developed at GKSS. It consist of measuring the relative displacement of two gauge points directly at the crack tip using special displacement gauges. The resulting CTOD is called δ_5 because the gauge length over which the CTOD isdetermined amounts to 5 mm (Figure 1). This technique is used for determining critical CTOD values as well as for deriving δ_5 crack growth resistance curves (Figure 2). The direct measurement of the CTOD has the advantage that no calibration function is needed as it is the case for the standard methodsand for the *J*-integral, and it can be applied to any specimen configuration. This way transferability studies can be easily performed.

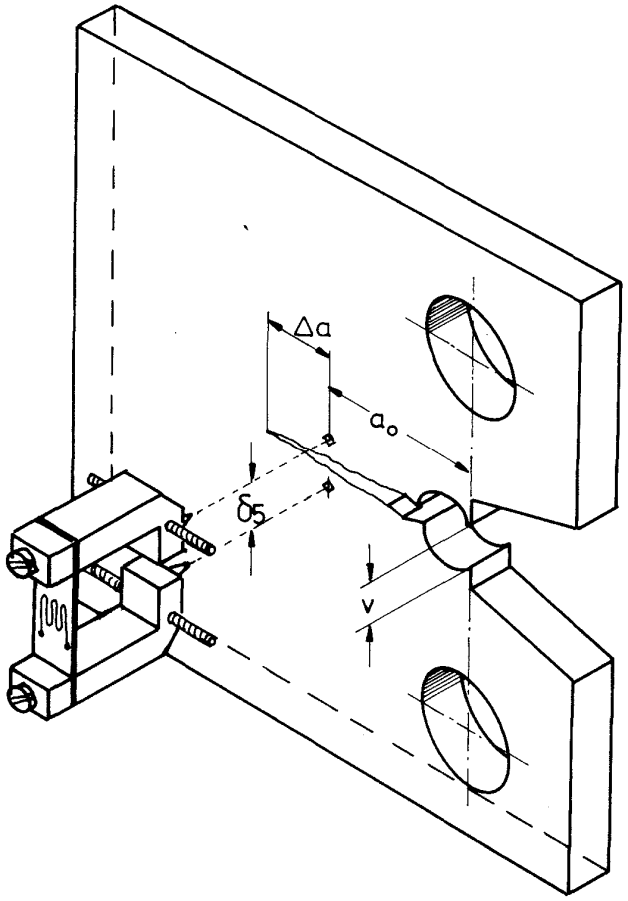

Figure 4.1 Method for determination of
Crack Tip Opening Displacement (CTOD)

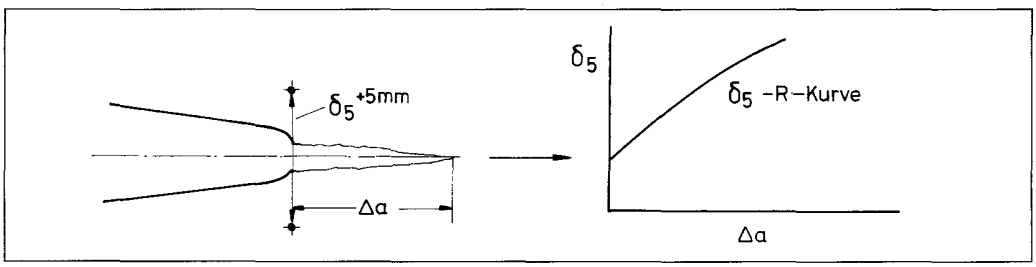

Figure 4.2 Determination of the CTOD R-Curve

4.2. Displacement Gauge For Small Working Ranges Up To 5 mm (δ_5-Compact-Clip)

In order to experimentally detemine δ_5, the δ_5-Clip is inserted into two Vickers hardness identations. The clip gauge is attached to the specimen by a simple lever setup which is pressed on the surface with a spring.

The clip gauge is connected to an amplifier. The deflection of the clip gauge caused by the crack tip opening displacement alters the balance in a Wheatstone bridge circuit. The signal is proportional to the displacement of the gauge points on the δ_5-Clip.

The δ_5-Compact Clip was particularly developed for determining the CTOD in the form of δ_5. Special fixtures are necessary for accomodating the clip gauge. They have to be adjusted to size and geometry of the specimen. The δ_5-Compact Clip can also serve for determining crack closure during fatigue crack propogation.

According to the test requirements the working range can be varied from 1 mm to 5 mm. Them measuring error is 0,5 % of the maximum value.

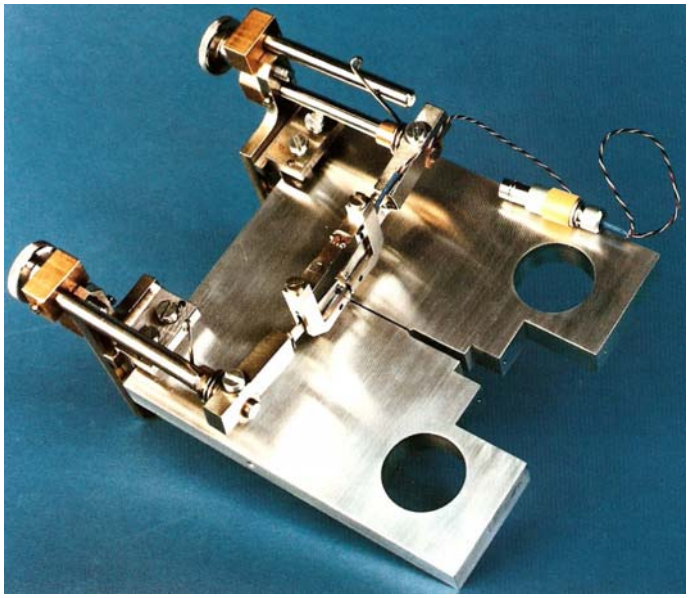

Figure 4.3 Application of the δ_5 clip gauge to a C(T) specimen

CHAPTER FIVE
MODELLING AND ANALYSIS OF C(T) SPECIMEN USING ABAQUS

5.1 Introduction

In thıs study, the C(T) specimen has been modeled using ABAQUS/CAE Version 6.6 software. In the following sections, modelling steps has been described. When ABAQUS/CAE has been started, the screen shown in Figure 5.1 appears.

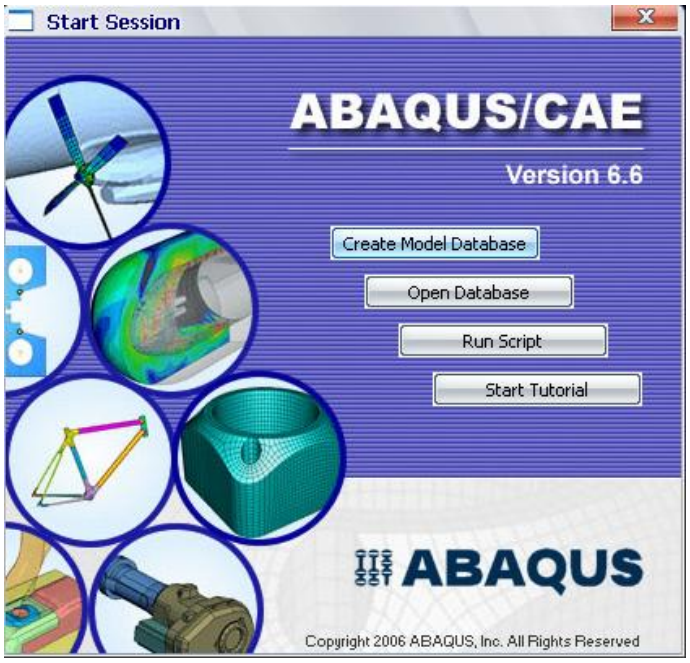

Figure 5.1. ABAQUS/CAE Version 6.6

5.2 Modelling Base Metal Specimen

In the beginning, a part has been created. To create a part, in the **Part** module **Model > Create** has been clicked. Then the window shown in Figure 5.2 appears. In this window, part name, modeling space, modeling type, options of modeling type, base feature and approximate size have been described.

In this study, **"Create Part Window"** for base metal has been filled as shown in Figure 5.2.

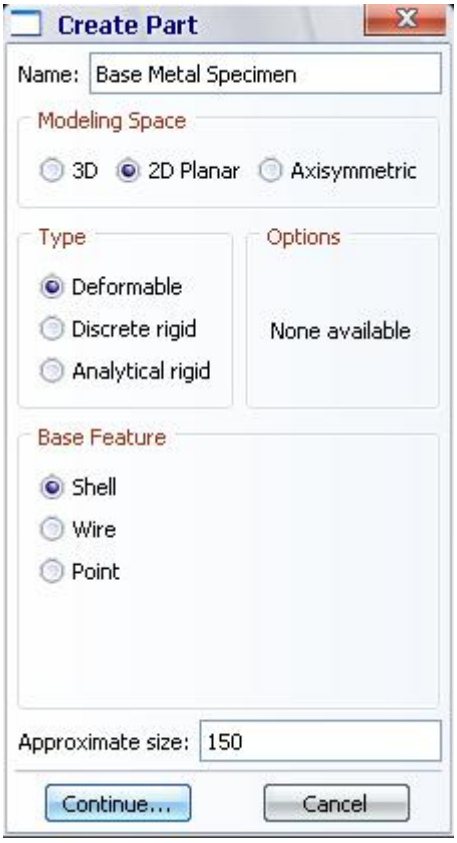

Figure 5.2. Create Part Window

After clicking continue, **"Sketch Screen"** has been opened. In this part, the C(T) Specimen model has been sketched. Sketch of this model is shown in Figure 5.3.

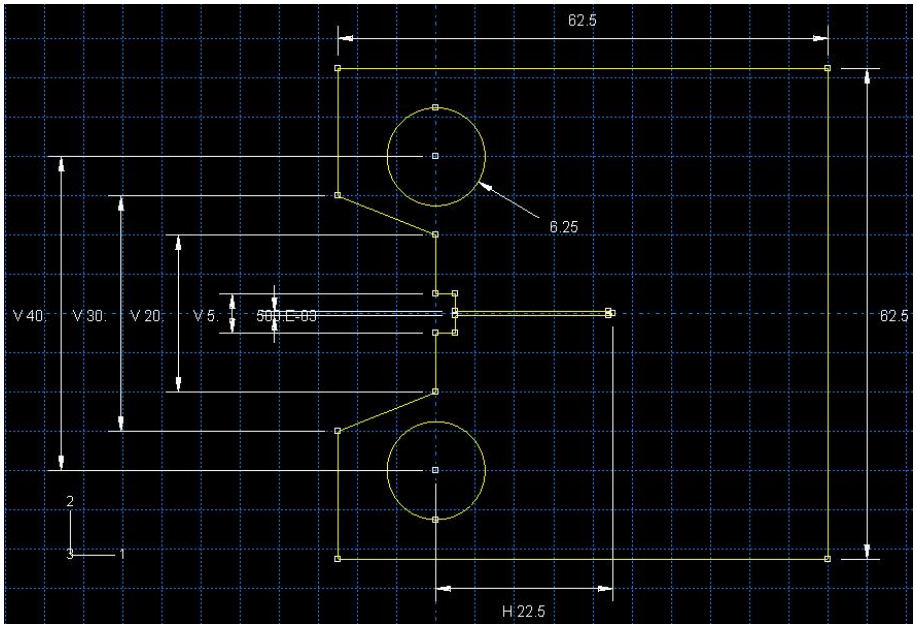

Figure 5.3 Sketch of C(T) Specimen For Base Metal

After sketching was completed, by clicking **"Done"** button, **"Edit Base Extrusion"** window has been opened. In this window, depth of the model and extrusion type were described. Then model has been created.

In fatigue tests there is a seam. That seam provide a crack that is assumed as the beginning of the fatigue crack. To create this zone, partition method was used from toolbar by clicking **Tools > Partition**. After partitioning, the model was completely created.

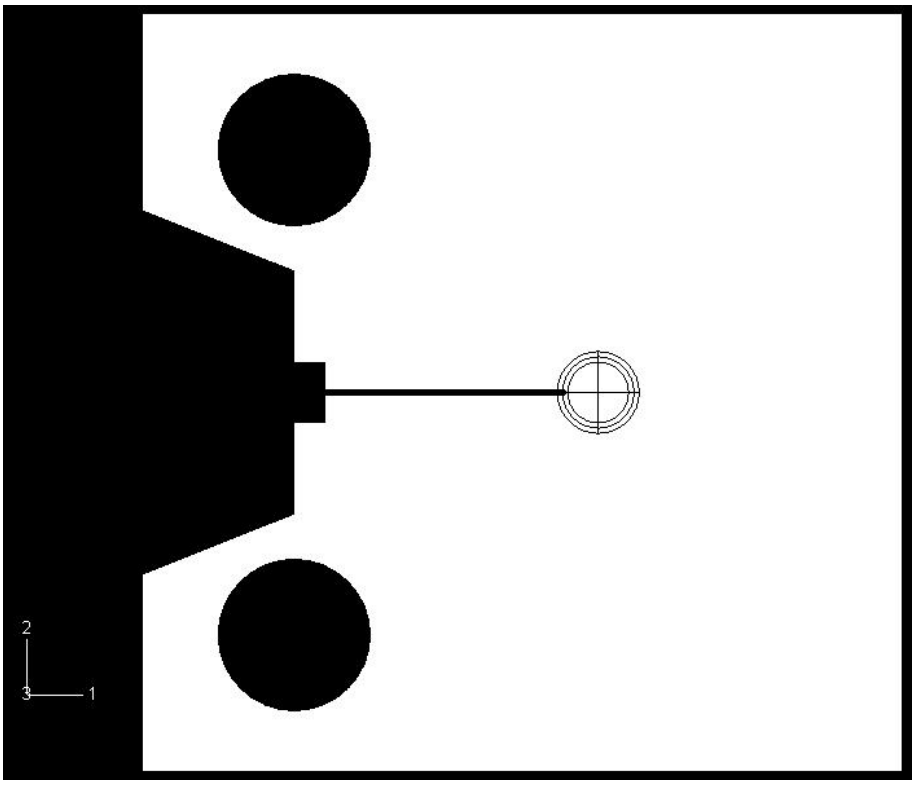

Figure 5.4. Partitioned Base Metal C(T) Specimen

After modelling, mechanical properties of aluminum have been described. In **Property** module by clicking **Material > Create "Edit Material"** window was opened. In this window, material name and properties (mechanical, thermal etc.) have been set. 6056 series aluminum alloy has been used for this study. Mechanical properties of this material were quoted from the stress – strain curve that is shown in Figure 5.5. This material has an elasto-plastic behavior. The curve of BM has been considered for this part of study.

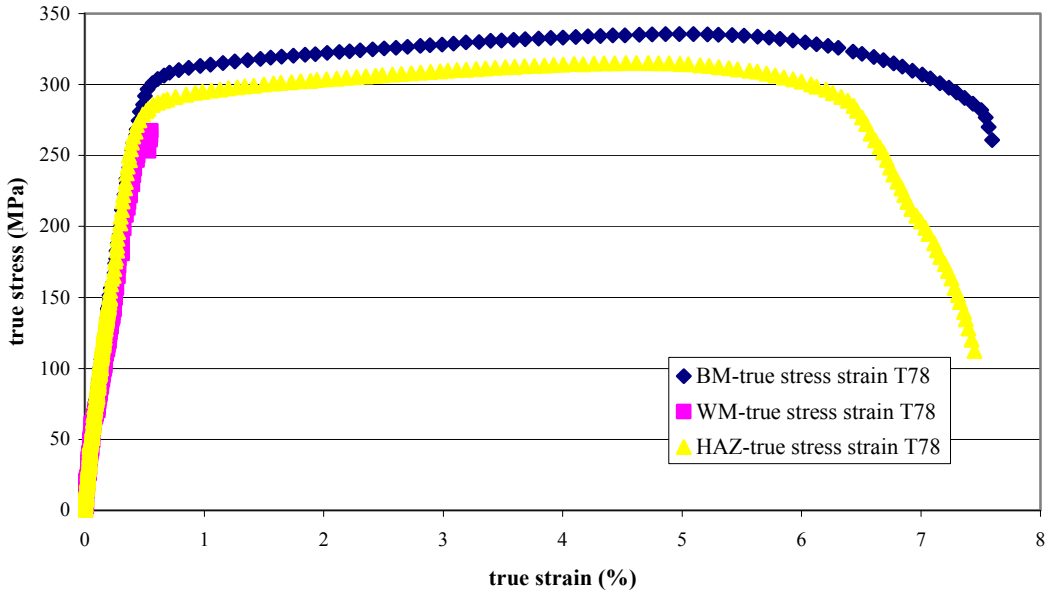

Figure 5.5. Stress – Strain Curve of 6056 Aluminum

Because of elasto-plastic behavior of material, properties have been set in two steps. First step has involved elastic properties that were "Young's Modulus" and "Poisson's Ratio". This step was done by clicking **Mechanical > Elasticity > Elastic** from the "Edit Material" window as shown in Figure 5.6.

The second step was done by clicking **Mechanical > Plasticity > Plastic** from the same window as shown in Figure 5.7. This property has involved "Yield Stress" and "Plastic Strain".

After setting material properties, for each material sections have been created by clicking **Section > Create**. Section was used to set the zone of material. In this part there was only one material, so only one section existed. Created sections were assigned to regions by clicking **Assign > Section**.

Last step of modelling consisted of assembly. In this step, the instances of the part have been created. In **"Assembly"** module by clicking **Instance > Create** the instances have been created. For this part instances have been created as independent.

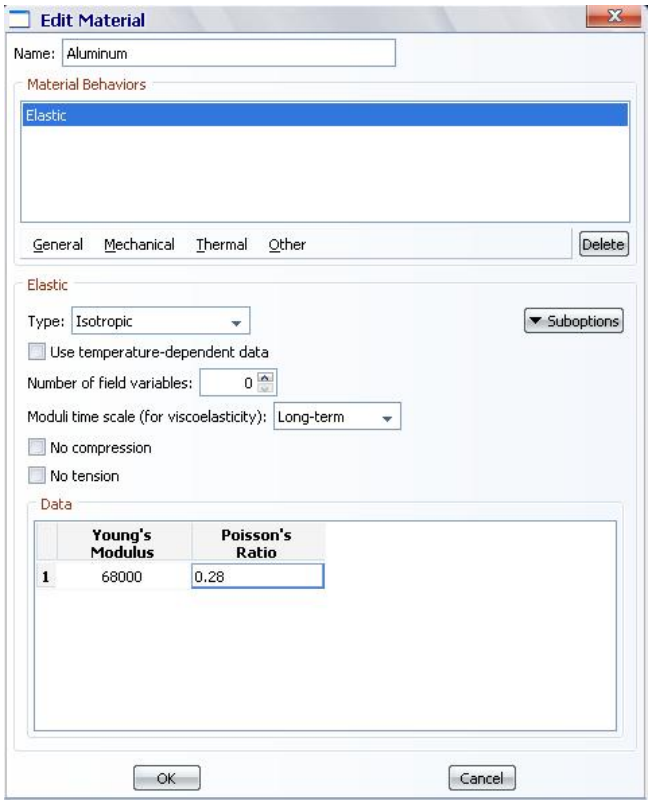

Figure 5.6. Elastic Properties of Material

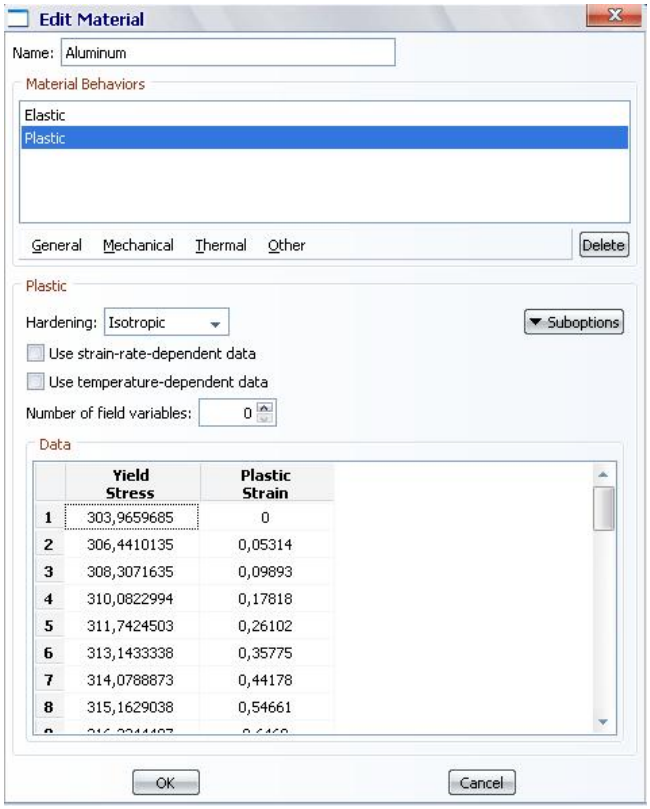

Figure 5.7. Plastic Properties of Material

After modelling the part, the pre-crack has been created. In **"Interaction"** module by clicking **Special > Crack > Assign Seam** the zone that seam occurred has been created. In this study, seam has been set on the partition zone as shown in Figure 5.8. Only in this module the seam appears evidently.

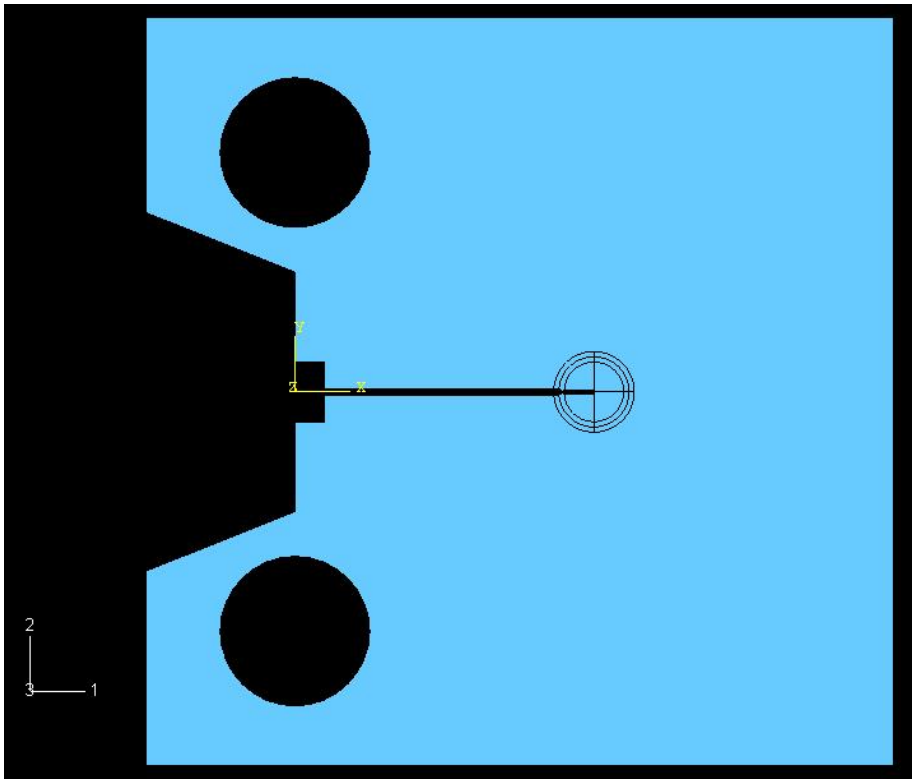

Figure 5.8. Assigned Seam

Assigning the seam is the first part of creating a crack. After assigning the seam, crack driving zone and direction were described by clicking **Special > Crack > Create**. In this step, crack front and direction have been set. Crack front has been marked by a green cross as shown in Figure 5.9.

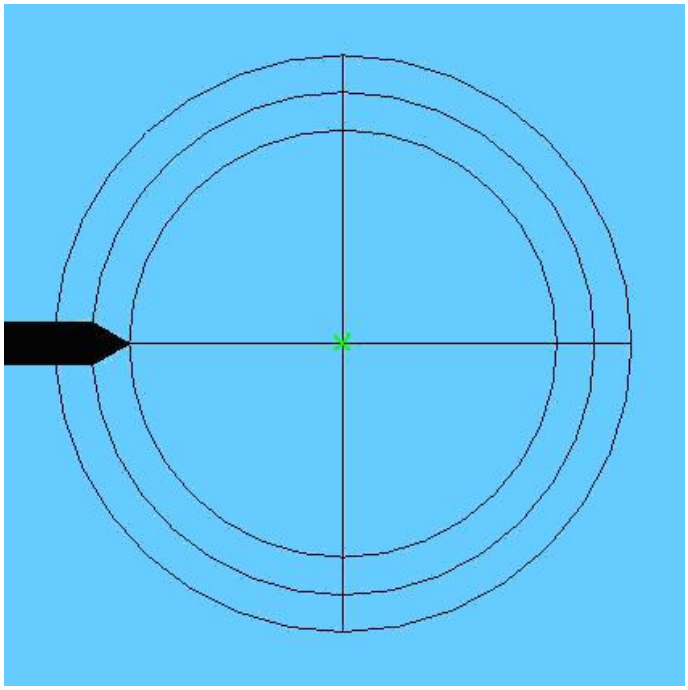

Figure 5.9. Crack Front

To analyse the model, analysis type and output data requests have been described in **Step** module by clicking **Step > Create**. In this study, static analysis has been chosen as the analysis type. Stress and displacement outputs were requested by clicking **Output > Field Output Requests > Create**. *J*-Integral output was requested by clicking **Output > History Output Request > Create**. In history output request screen, output type was chosen as contour integral and number of contours have been set as 10. This screen is shown in Figure 5.10. Thus, the results that were requested have been described.

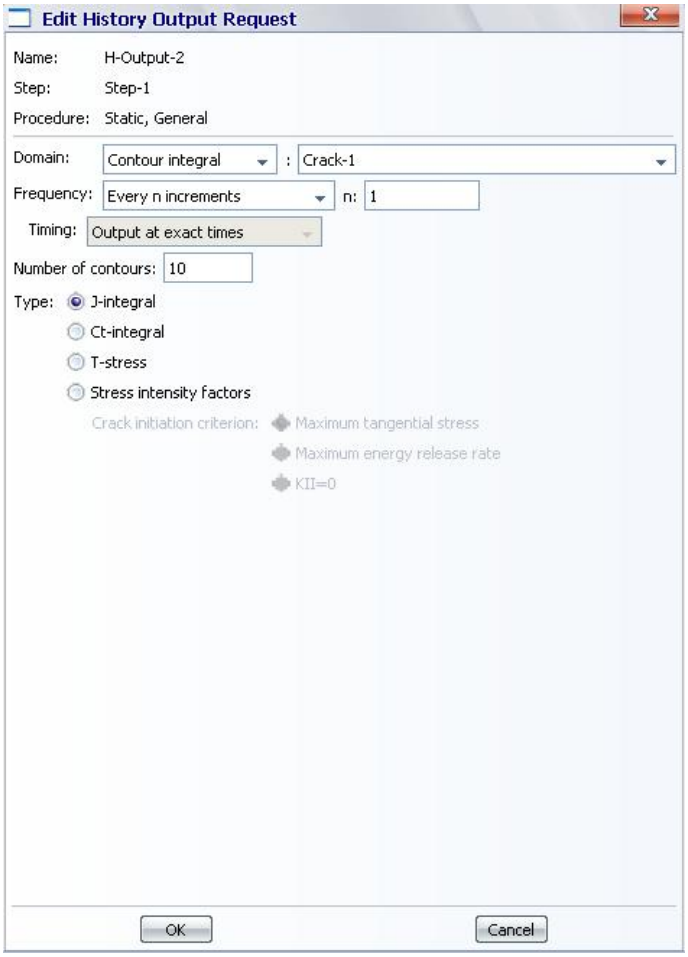

Figure 5.10. History Output Request Screen For *J*-Integral

Over all these steps, part was ready to be analysed by applying load. In this analysis, load has been applied to holes in opposite directions. Before loading, reference points that loads have been applied on them were set by clicking **Tools > Reference Point**. These points were set in the middle of each hole.

This model had a load type of concentrated force. Applying loads was done on **Load** module by clicking **Load > Create**. Load type has been chosen, then amount and direction of the loads have been set on "Edit Load" window. This window is shown in Figure 5.11.

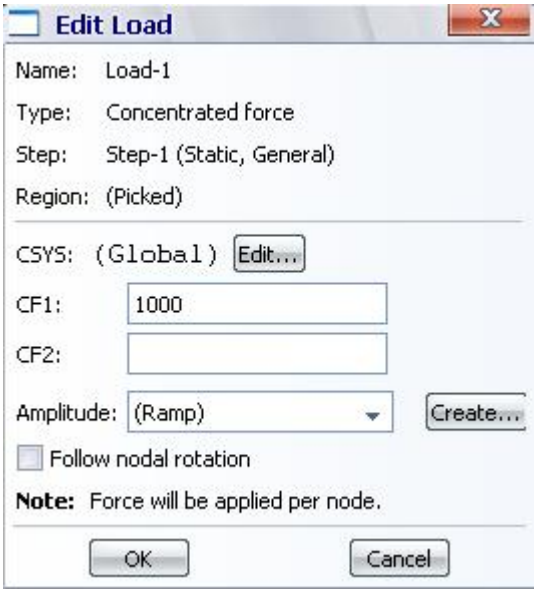

Figure 5.11. "Edit Load" Window

Application of the loads to the part are shown in Figure 5.12.

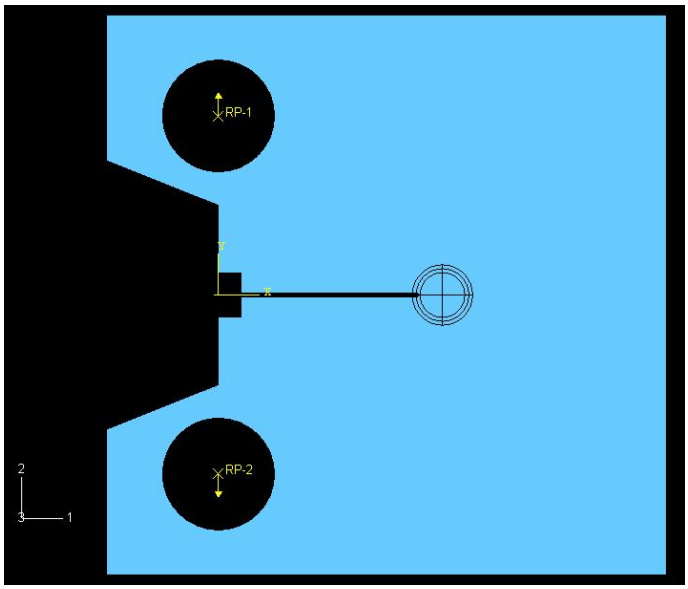

Figure 5.12. Loaded Model

Before running the analysis, last step was meshing. Meshing is one of the base functions of CAE softwares which uses finite element method. In this model, mesh size has been related to measurements of part and analysis sensitivity. Mesh size has been set on **Mesh** module by clicking **Seed > Edge By Size**. Then the region to be

meshed was chosen and mesh size has been set. After setting the mesh size, part has been meshed by clicking **Mesh > Part**. Meshed part is shown in Figure 5.13.

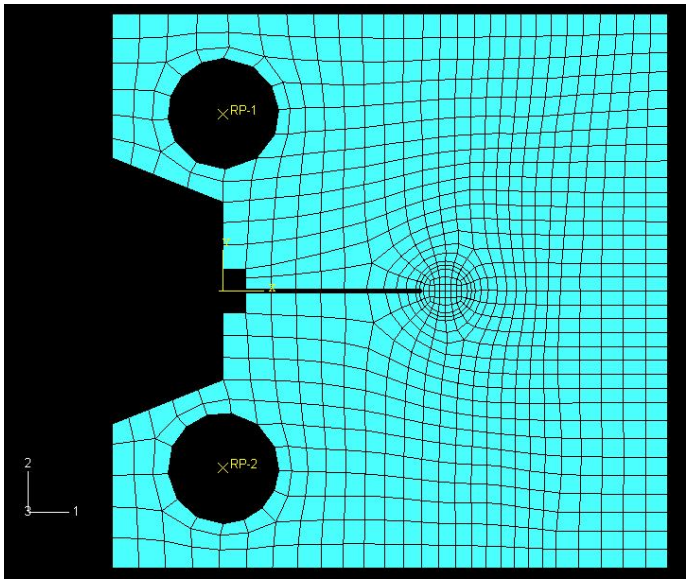

Figure 5.13. Meshed Model

After meshing, part was ready to analyse. In **Job** module, a job has been created to run the analysis by clicking **Job > Create**. Default settings were used in this model. Analysis has begun after clicking submit button in job screen.

Analysis results have been plotted or printed in **Visualization** module. Deformed shape, undeformed shape or both could be plotted by clicking **Plot > Deformed Shape** or other sub-options. Output requests could be printed by clicking **Report > Field Output**.

Deformed shape of this model is shown Figure 5.14. This shape is related to Von Mises stress method.

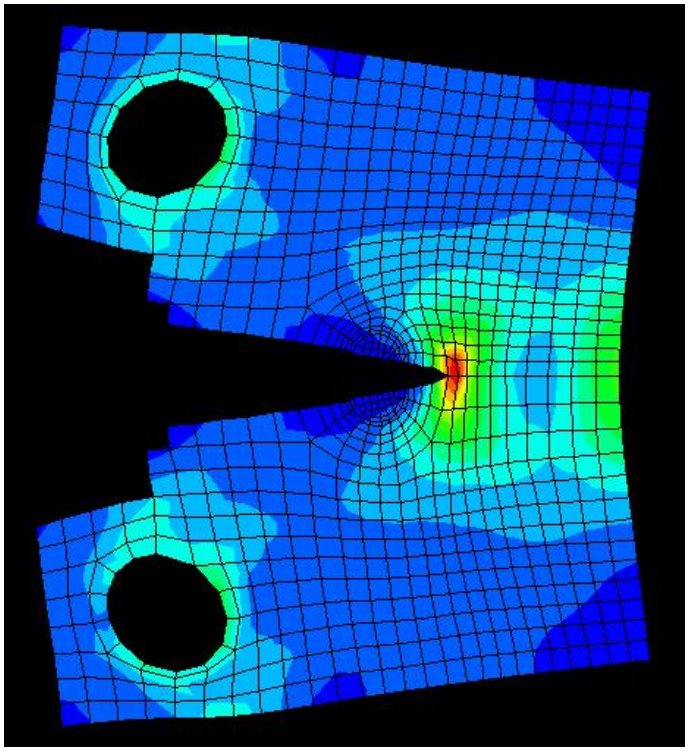

Figure 5.14. Deformed Base Metal C(T) Specimen

5.3 Modelling of The Specimen With A Crack In Weld Region

This model had the same size as the Base Metal Specimen. The crack was created in the weld region. There were nearly 2 mm thick weld zone and 1.5 mm thick heat affected zone on both sides of the weld zone. Partition of the model was regenerated according to these zones. Figure 5.15 shows this model's partition.

After partitioning, new materials have been described for the weld zone and the heat affected zone. Therefore, new sections were created and assigned. This specimen was modeled same as the Base Metal Specimen except those settings. Results of these model analyses are shown in Figure 5.16.

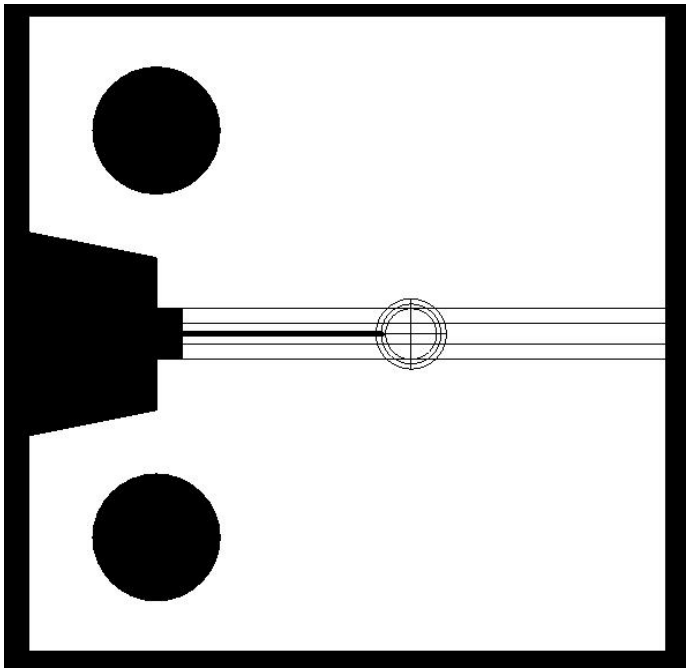

Figure 5.15. Partitioned Weld Metal C(T) Specimen

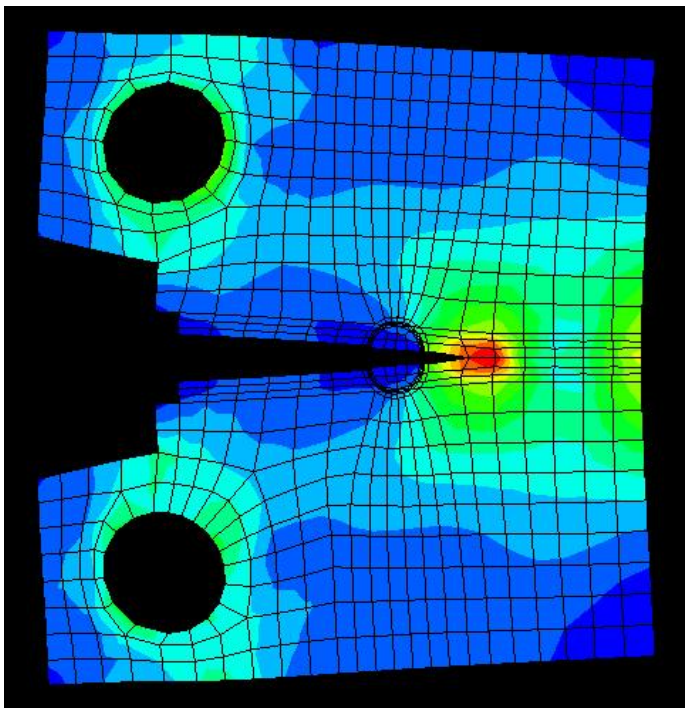

Figure 5.16. Deformed Weld Metal C(T) Specimen

5.4 Modelling of The Specimen With A Crack In The Heat Affected Zone

This model also have the same size as other specimens. Weld zone and heat affected zone have been placed axsymetrically. Crack growth direction was between the weld zone and the heat affected zone. Thus, partitioning of this model is as shown in Figure 5.17.

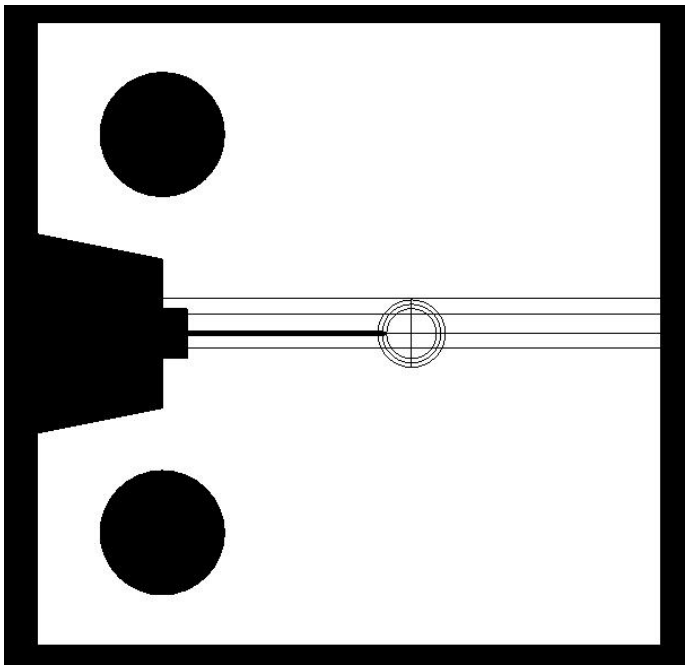

Figure 5.17. Partitioned Heat Affected Metal C(T) Specimen

Model has been analysed with the same boundary conditons, loads and materials. Deformed shape result is shown in Figure 5.18.

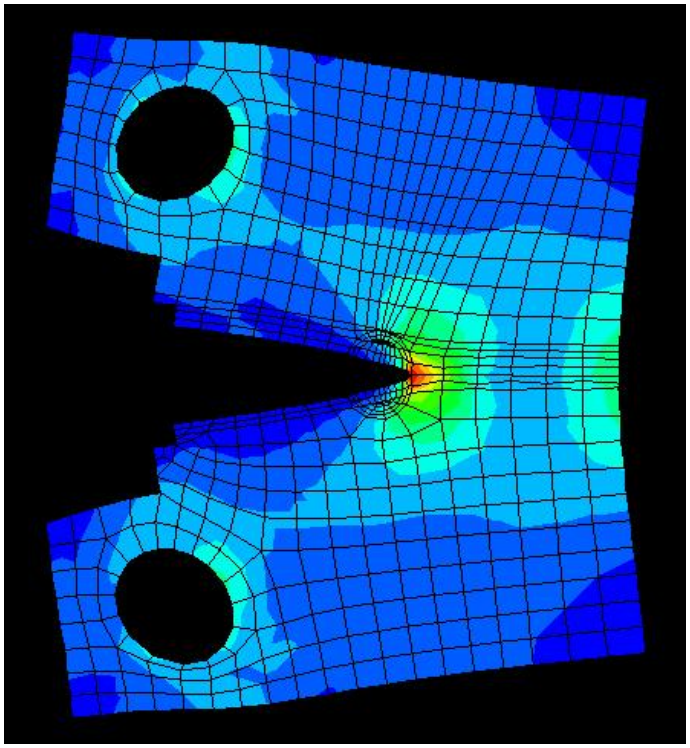

Figure 5.18. Deformed Heat Affected Metal C(T) Specimen

J-Integral results are obtained from History Output Request option. The fifth contour result was used as in agreement with literature.

CHAPTER SIX
RESULTS AND DISCUSSION

In this study, ABAQUS/CAE 6.6.1 was used to determine the crack growth and fracture behavior of welded mis-matched joints. Experimental results were compared to analytical results.

Three type of specimens, which were made of 6056 series aluminum alloy were used in this study, namely, base metal specimen, welded specimen with crack in the weld region and welded specimen with crack in the heat affected zone. *J*-Integral criterion and *R*-Curve approach were used to obtain the fracture behavior results.

Analysis results have been presented and discussed in this chapter. Comparing the experimental results and numerical results, is the main purpose of this study. Three type of graphics are presented: CTOD – CMOD, CTOD-Δa, J-Δa, the last are named as R-curve or Resistance-Curve graphics, which indicate the crack growth resistance of a material with a crack. Experimental and numerical results have been shown on the same graphic in order to compare the suitability of the numerical analysis. These graphics have been designed for each model: Base Metal, Weld Metal, Heat Affected Zone. CTOD – CMOD graphics are shown in Figure 6.1, Figure 6.2 and Figure 6.3.

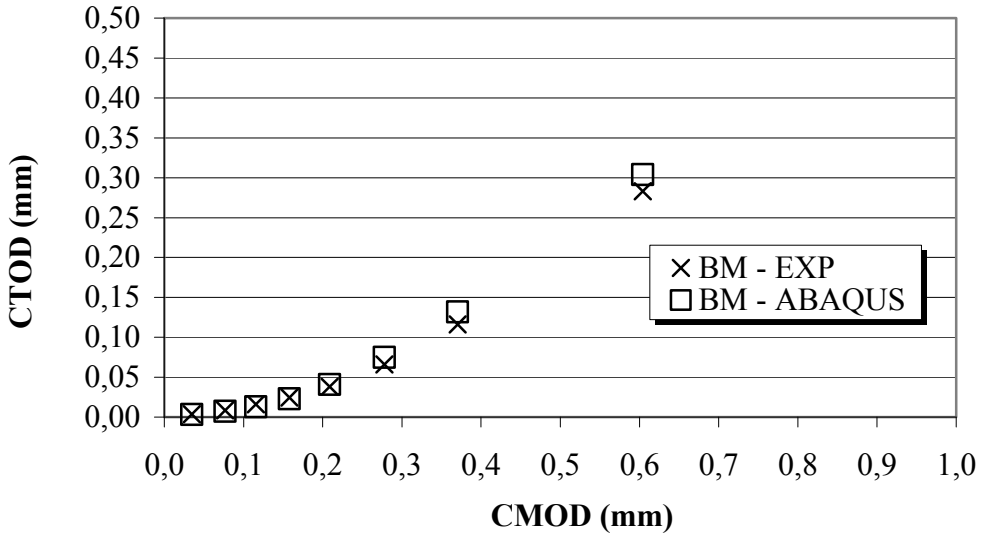

Figure 6.1. CTOD – CMOD Graphic of Base Metal Specimen

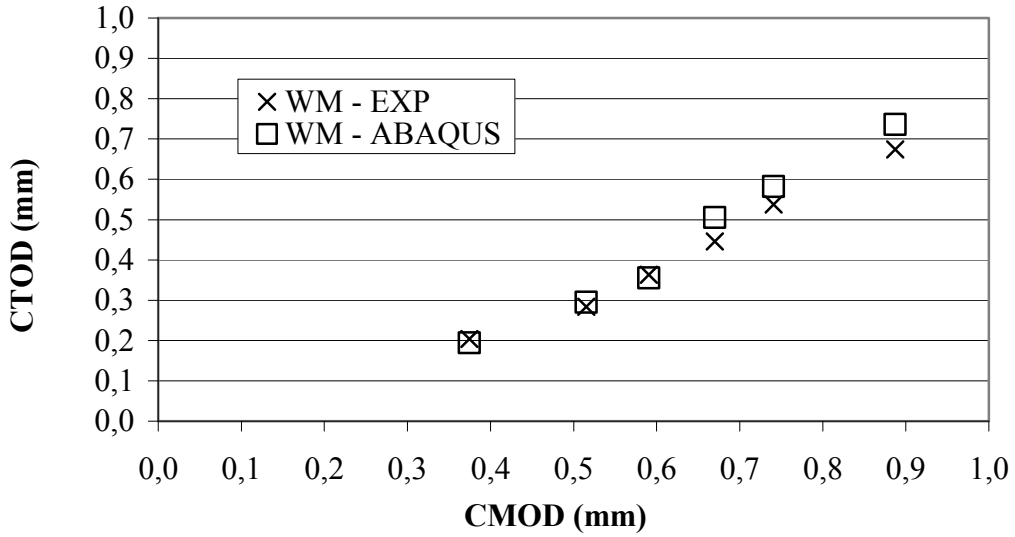

Figure 6.2. CTOD – CMOD Graphic of Weld Metal Specimen

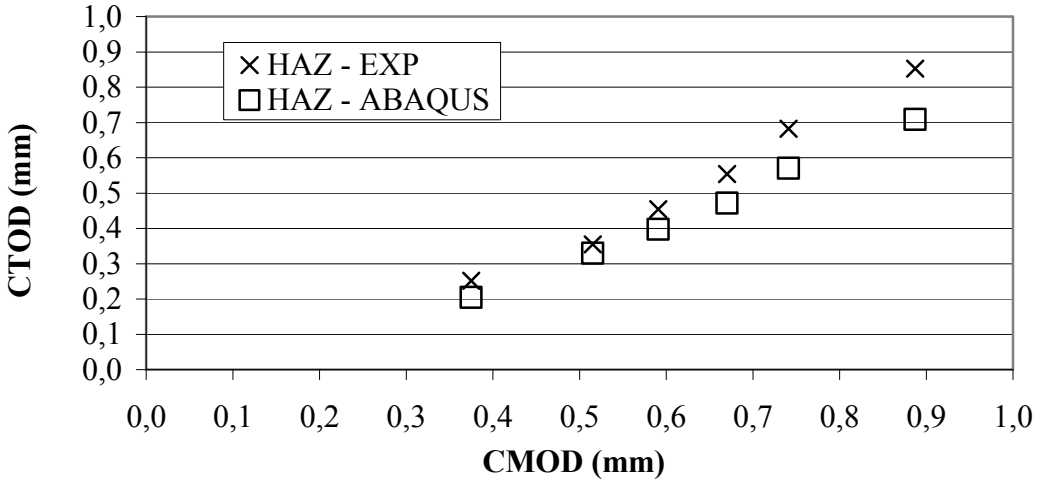

Figure 6.3. CTOD – CMOD Graphic of Heat Affected Zone Specimen

As seen from the CTOD-CMOD curves, the ratio of CTOD/CMOD is converges to about 0.5 as the values increase in Base Metal (BM) specimen. For Weld Metal (WM) and Heat Affected Zone (HAZ) specimens this ratio is seen to be greater, the ratio of HAZ being greater than WM specimen. The reason for this could be that since the mechanical properties of the BM are higher than the other two conditions. Therefore it is harder for the propagating crack to open laterally under the applied load. Whereas, in the other types, since the mechanical properties are lower compared to the BM, it is easier for the crack to propagate into the metal. Therefore, the ratio of CTOD/CMOD is higher.

CTOD – Δa (R-curve) graphics of all three specimens are shown in Figure 6.4, Figure 6.5 and Figure 6.6.

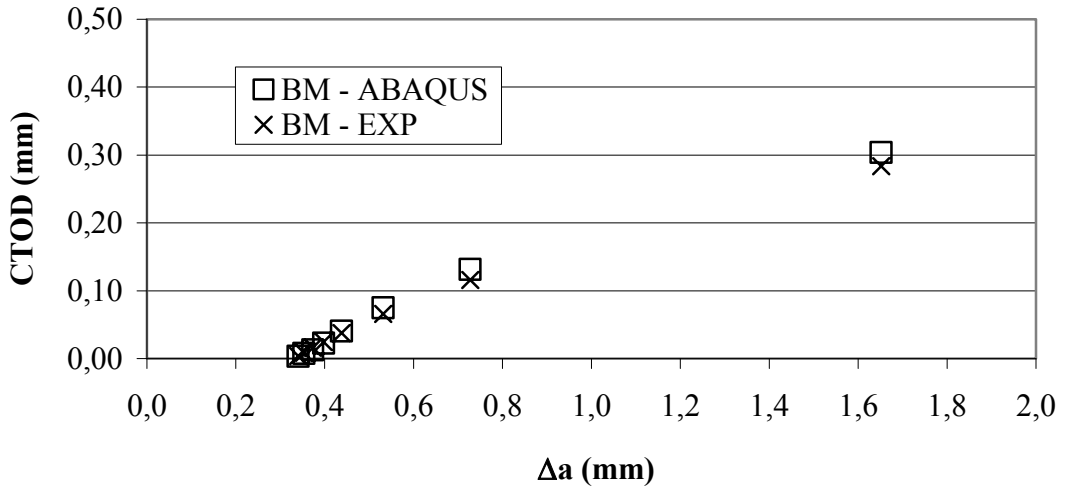

Figure 6.4. CTOD – Δa Graphic of Base Metal Specimen

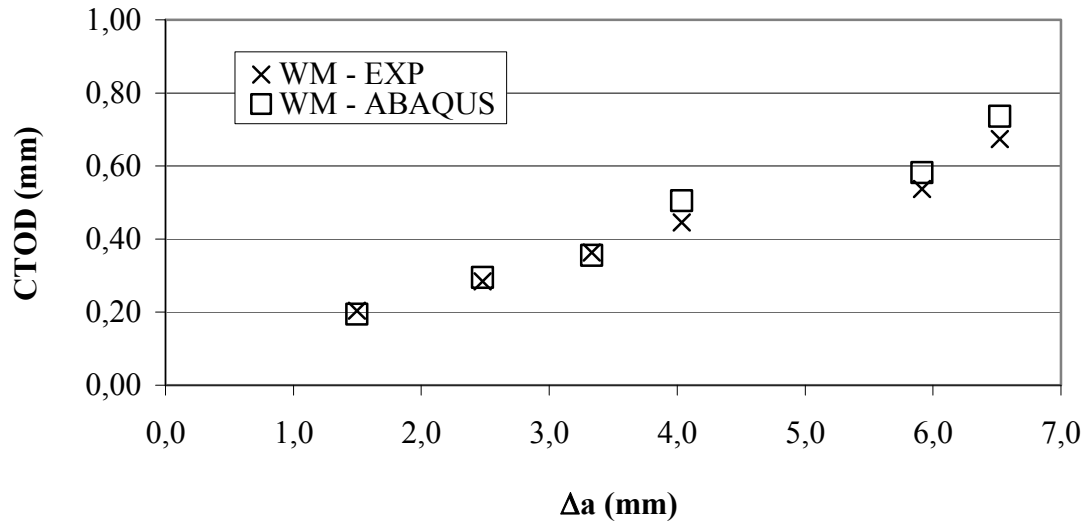

Figure 6.5. CTOD – Δa Graphic of Weld Metal Specimen

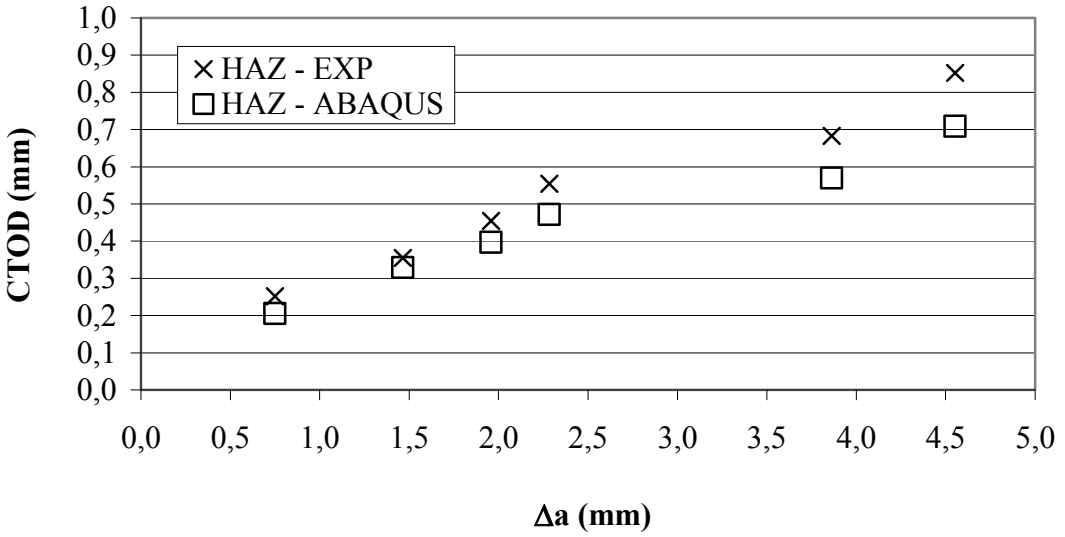

Figure 6.6. CTOD – Δa Graphic of Heat Affected Zone Specimen

J – Δa (R-curve) graphics of both three specimens are shown in Figure 6.7, Figure 6.8 and Figure 6.9.

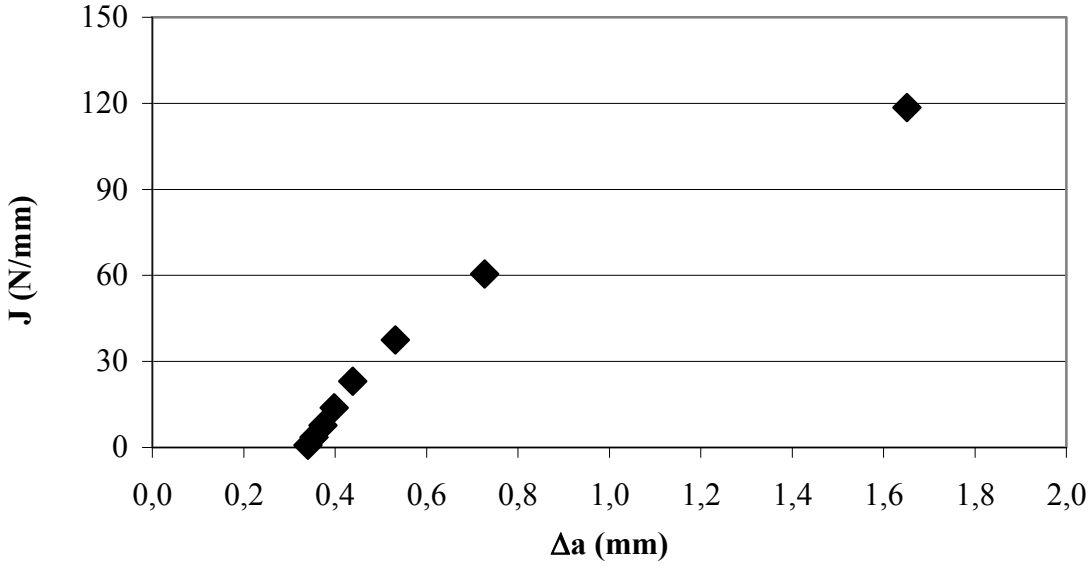

Figure 6.7. *J* – Δa Graphic of Base Metal Specimen

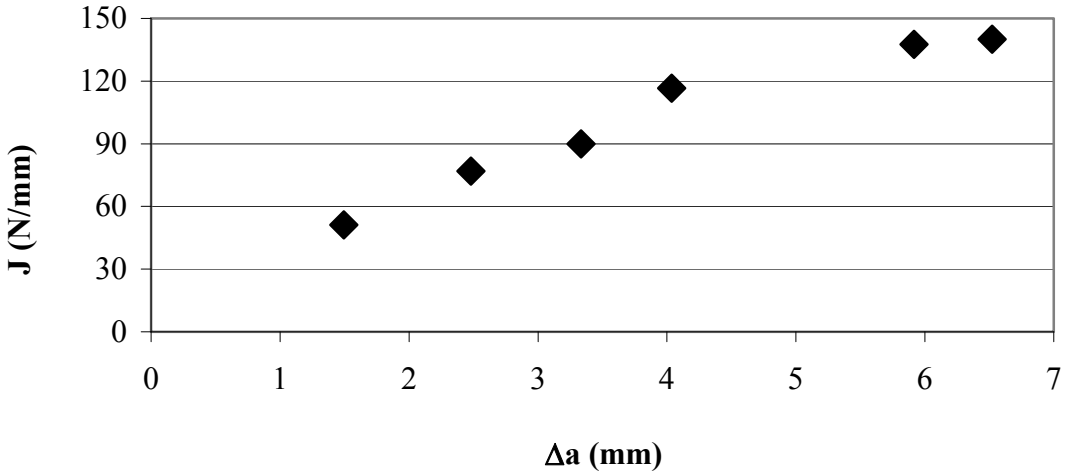

Figure 6.8. *J* – Δa Graphic of Weld Metal Specimen

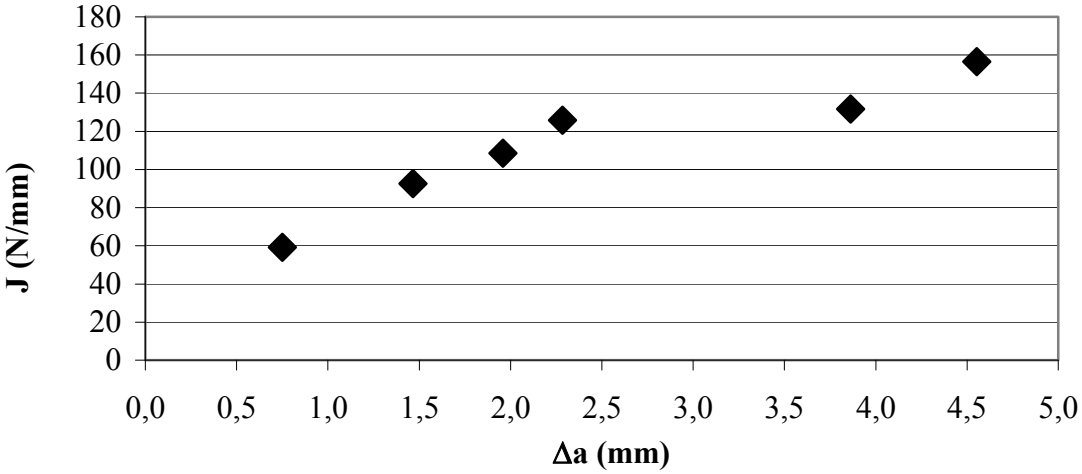

Figure 6.9. *J* – Δa Graphic of Heat Affected Zone Specimen

The graphics indicate the crack propagation resistance of the three types of specimens. The BM specimens yield a higher crack resistance, as seen from CTOD-Δa and J-Δa graphics, the crack extension is much lower in BM specimens compared to the other types. The lowest resistance is seen in WM specimens, since their mechanical properties are the lowest among the three conditions.

As seen from the graphics, experimental and numerical results are in good agreement. Therefore, it can be said that the software ABAQUS is a suitable analysis tool for fracture mechanics calculations.

CHAPTER SEVEN
CONCLUSIONS

The following facts can be deduced from this study:

- Laser beam welded AA 6056 plates have been used to obtain C(T) specimens for fracture mechanics analysis.
- Three types of C(T) specimens have been used, namely BM, welded specimen with crack in the WM and welded specimen with crack in the HAZ.
- Fracture mechanics test have been carried out in order to determine the CTOD, CMOD and Δa values corresponding to the applied load.
- ABAQUS software has been utilized to carry out the numerical analysis. The input parameters were the applied load and the crack length. The output parameters were CTOD, CMOD and J-integral.
- Experimental and numerical results have been compared with various graphics, it can be concluded that they are in good agreement for all conditions.
- It can be said that ABAQUS software is a suitable analysis tool for fracture mechanics analyses.
- As shown in J-Δa graphics J-Integral values of welded specimen with crack in the HAZ are higher than welded specimen with crack in the WM, and BM specimen has a lower value than WM. This J-Integral value difference is because of physical properties of each zone.

REFERENCES

Aluminium - Specifications, Properties, Classifications and Classes, Supplier Data by Aalco, Retrieved June 27, 2008, from *http://www.azom.com/details.asp?ArticleID=2863*

Anderson, T.L. (1995). *Fracture Mechanics: Fundamentals and Applications* (2nd Edition). Washington D.C; CRC Press

Begley, J.A. and Landes, J.D. (1972). *The J-integral as a Fracture Criterion*, "Fracture Toughness", ASTM STP 514, (1-20)

Bolm S. (1980). *Laser Welding Article, Laser Welding*, Cutting and Drilling, Retrieved April 22, 2008, from US LASER CORP database

Broek, D. (1982). *Elementary Engineering Fracture Mechanics* (3rd Edition). Boston; Martinus Nijhoff.

BS 5762 : 1979, *British Standard Methods for Crack Opening Displacement (COD) Testing*, London; British Standards Institute.

Christiansen, H.F. *GKSS – Displacement Gauge Systems for Applications in Fracture Mechanics* (1st Edition). Geesthacht: GKSS -lForschungszentrum Geesthacht GmbH.

Classification of aluminum alloys [SubsTech], Retrieved June 27, 2008, from *http://www.substech.com/dokuwiki/doku.php?id=classification_of_aluminum_alloys*

Heyer, R.H. and McCabe, D.E. (1972). *Plane-Stress Fracture Toughness Testing Using a Crack-Line-Loaded Specimen*, Engineering. Fracture Mechanics (Vol.4), (393-412)

Hood, J.E. (1971). *Fracture Initiation in Tough Materials*, Conf. of Metallurgists, CIMM, Montreal.

Irwin, G.R. & Kies, J.A. (1954). *Critical Energy Rate Analysis of Fracture Strength*, Welding J. Research Supplement, (Vol.19), (193 – 198).

Naeem, M. & Jessett, R. (2001). *Welding Aluminum Tailored Blanks with Nd:YAG Lasers for Automotive Applications*, Practical Welding Today, Retrieved April 25, 2008, from http://www.thefabricator.com/ database

Neale, B.K. & Heerens, J. (1994). *The GKSS Test Procedure For Determining The Fracture Behaviour of Materials EFAM GTP 94* (1st Edition). Geesthacht: GKSS -lForschungszentrum Geesthacht GmbH.

Paris, P.C. (1977). *Fracture Mechanics in the Elastic-Plastic Regime*, "Flaw Growth and Fracture", ASTM STP 631, (3-27).

Rice, J.R. (1968). *A Path Independent Integral and the Approximate Analysis of Strain*, Concentrations by Notches and Cracks, J. Applied Mechanics, Trans. ASME, (Vol.35), (379-386).

Wells, A.A. (1961). *Unstable Crack Propagation in Metals - Cleavage and Fast Fracture*, Cranfield Crack Propagation Symposium, Vol.1, 210.